

# Prescient teleoperation of humanoid robots

Luigi Penco<sup>1</sup>, Jean-Baptiste Mouret<sup>1</sup>, Serena Ivaldi<sup>1</sup>

<sup>1</sup> Inria Nancy – Grand Est, CNRS, Université de Lorraine, France

serena.ivaldi@inria.fr

Humanoid robots could be versatile and intuitive human avatars that operate remotely in inaccessible places: the robot could reproduce in the remote location the movements of an operator equipped with a wearable motion capture device while sending visual feedback to the operator. While substantial progress has been made on transferring (“retargeting”) human motions to humanoid robots, a major problem preventing the deployment of such systems in real applications is the presence of communication delays between the human input and the feedback from the robot: even a few hundred milliseconds of delay can irreversibly disturb the operator, let alone a few seconds. To overcome these delays, we introduce a system in which a humanoid robot *executes commands before it actually receives them*, so that the visual feedback appears to be synchronized to the operator, whereas the robot executed the commands in the past. To do so, the robot continuously predicts future commands by querying a machine learning model that is trained on past trajectories and conditioned on the last received commands. In our experiments, an operator was able to successfully control a humanoid robot (32 degrees of freedom) with stochastic delays up to 2 seconds in several whole-body manipulation tasks, including reaching different targets, picking up, and placing a box at distinct locations.

## Introduction

Humanoid robots are some of the most versatile machines ever created [1]. Thanks to their anthropomorphism, they can perform bimanual manipulation like grasping large boxes, they can bend to pick up objects from the ground, or reach high places by the ceiling; they can also walk on rough terrains, crawl, climb stairs or push objects. By contrast with quadrupeds, their kinematic structure allows them to enter narrow or cluttered spaces, and operate in environment that were primarily designed for humans. In short, humanoid robots have the potential of being as versatile as humans, being currently limited only by their mechatronics, which needs to be further developed to match the human flexibility.

This versatility is especially important when robots are sent to truly unexpected situations in which they have to perform a task for which they were not designed [2]. Hence, while robots in the manufacturing industry perform well-defined tasks in known environments, many situations in the outside world involve some creative adaptation of the tasks. For instance, disasters — natural or industrial — are events that are, by definition, out of the ordinary routine, and during which robots could be critical to save lives. Similarly, working in remote places like in space or on an oil platform very often requires performing tasks in unexpected ways.

Nevertheless, autonomous robots are far from being the creative problem solvers that humans are; this is why humanoid robots are most useful when they are teleoperated [2, 3]: the capabilities of the robot and of the operator are combined to solve complex problems remotely. While humanoid robots can be operated from high-level commands and classic joysticks [3], they can exploit their human-like morphology to directly replicate the human posture and gestures, captured by a motion tracking system. This technique coupled with the intelligence of the human operator makes them realize tasks fluently as human avatars. With such a *whole-body teleoperation*, the entire body of the robot can be controlled precisely and the human operator with a virtual reality headset may feel like been “projected” to the remote situation. Additionally, there is a good match between teleoperation and humanoid robots because they are typically considered for high-value missions (life-or-death situations, nuclear accidents, ...) for which the wage of an operator is negligible, but the stakes are too high to let a robot decide everything by itself.

Two main challenges are raised by humanoid teleoperation: (1) how to map a whole-body motion of the human to a robot that has close, but different physical constraints and dynamics [4, 5]? and (2) how to cope with the unavoidable communication delays between the movement of the operator and the feedback? The present paper addresses these two challenges but it is focused on delay compensation because substantial work has already been achieved for whole-body retargeting [4, 6].

The first studies with robot manipulators [7], suggested that the typical user behavior in a teleoperation system with time delays is to adopt a “move-and-wait” strategy to avoid overcompensations of the delayed perceived errors. However, follow-up experiments [8] showed that this strategy is not effective, even with time delays around 0.3s. This is in sharp contrast with the typical delays that are considered in real applications, for instance 1 second on average (30 s maximum) during the DARPA Robotics Challenge [2], 10 seconds (20 s maximum) for

the NASA Space Challenge [9], or 0.8 seconds (3 second maximum) in the METERON project [10], during which a robot was teleoperated on Earth from the International Space Station.

Time-delayed teleoperation almost exclusively use *predictive displays* [11, 12], which are virtual displays representing a model of the robot and its environment, to compensate for the delayed visual feedback. In these systems, the operator performs the task on the display, controlling the simulated robot without any time delay, while sending the same commands — which will be delayed — to the real robot. More complex predictive displays overlay the predicted graphics to the delayed video [13, 14], which can be achieved by identifying a model of the environment and transmit it back to the operator side [14]. However, in most cases, the predicted graphics and the delayed video signals are kept in different displays, due to the difficulty of mixing video and graphics with enough quality and robustness. In all these cases, since perfect modeling is impossible, there is always going to be a difference between the real and modeled environment, which has to be coped by some local robot autonomy. Hence, these techniques just offer approximate cues until the actual feedback information is available, and should be considered as support tools rather than solutions on their own.

Here, we introduce a novel teleoperation systems in which the operator gets a synchronized video feed of *real images*, even when the communication channel imposes a 1 to 2 seconds delay.

Our key idea is that if the robot executes the desired movement *before* the operator performs it, then the operator will watch a delayed video feed that will be almost indistinguishable from a real-time feed. At each time-step, the robot analyzes the data that it has received so far, measures the communication time, estimates the communication time to send the feedback, and predicts what the operator is most likely to do in the next seconds. This prediction makes it possible to execute the command with enough anticipation so that the user receives a video feed that correspond to the past of the robot, but that matches the present time for the operator. We call this prediction-based feedback scheme *prescient teleoperation*.

## Results

We use the humanoid robot iCub [15, 16], which has 32 degrees of freedom (ignoring the hands and the eyes) controlled in position (Method). The whole-body motion of the robot is defined by the trajectories of the center of mass ground projection, the waist height, the hands positions, and the posture of the arms, of the neck and of the torso. Each of these trajectories has a different priority which determines how the robot’s controller executes the entire movement (Methods): the top priority is given to the center of mass (to avoid falling) and the feet poses (which should not move in our experiments, since we only target double support motions), and the postural trajectories have the lowest priority. The exact hard and soft priorities were found in previous work with a multi-objective stochastic optimizer so that the robot is unlikely to fall but tracks the trajectories as well as possible [5].

At each time-step (100 Hz), the robot searches for the joint positions by solving a hierarchical constrained quadratic problem with inequality and equality constraints [17, 18] (Methods) that minimizes the tracking error while taking into account the priorities and the constraints (joint

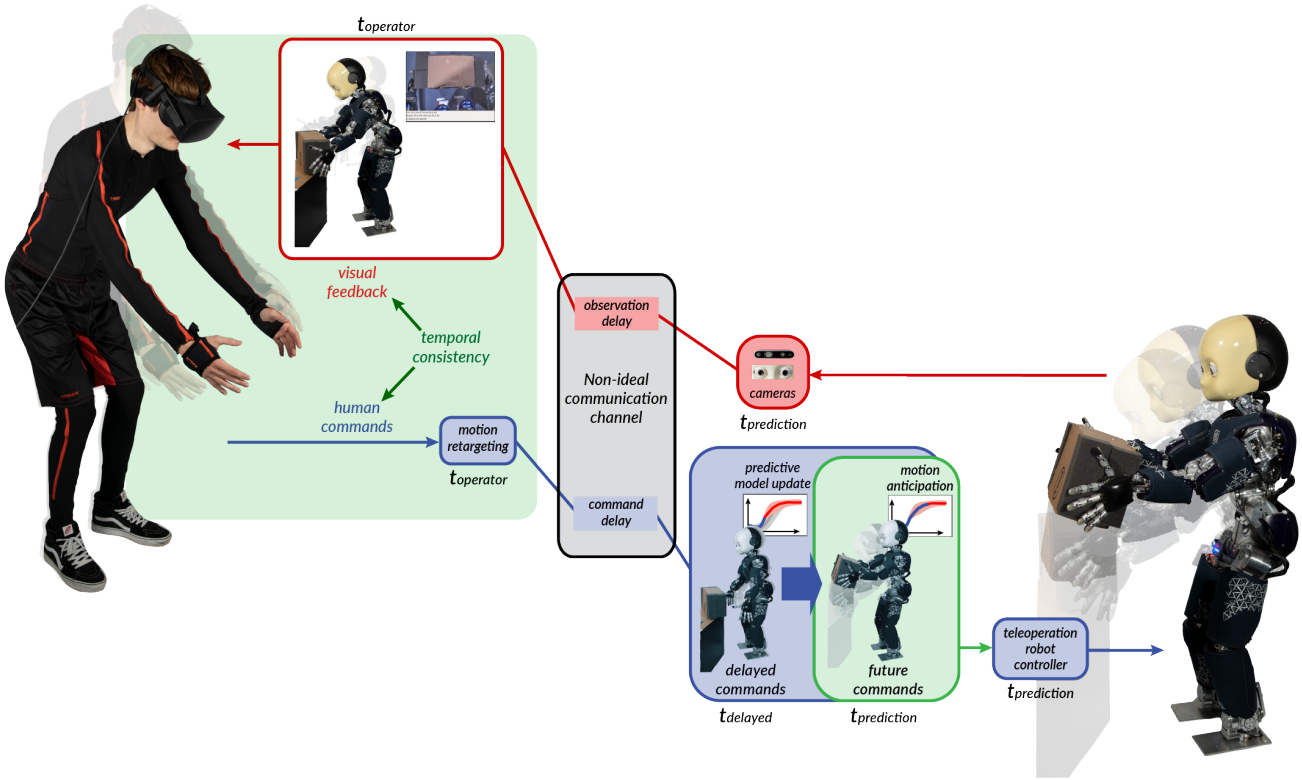


**Fig. 1. Concept of prescient teleoperation.** The operator wears a motion capture suit and a virtual reality headset. They teleoperate a humanoid robot over a network with communication delays (up to 2 seconds). To send a synchronized visual feedback to the operator, the robot *anticipates* the commands thanks to data-driven predictors that are trained from a few examples beforehand: the robot executes commands that the operator has not given yet by predicting the most likely commands in the next seconds.

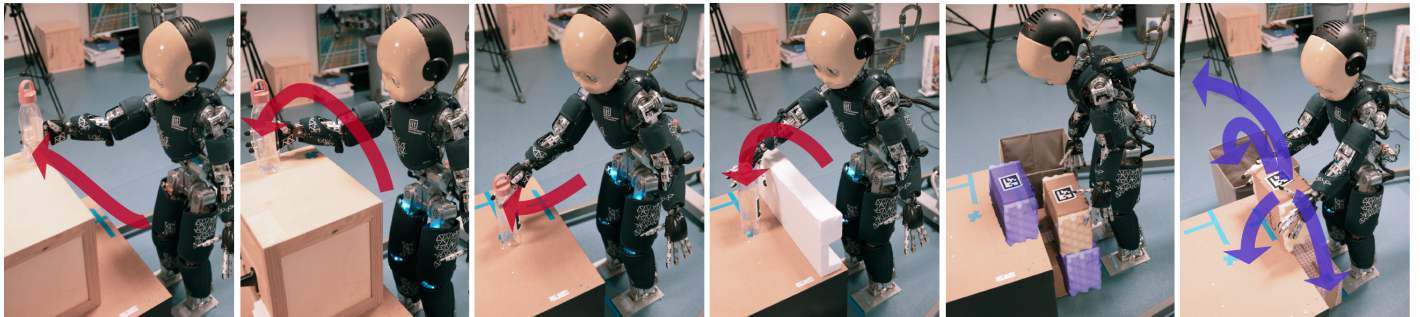


**Fig. 2. Tasks performed by the robot during the experiments.** In the first scenario (4 left images), the robot is teleoperated to reach a bottle at different locations and in different ways; in the second scenario (2 right images), the robot has to pick up a box from different locations then place it in another location.

velocities and zero moment point bounds). The tracking accuracy of this controller is reported in supplementary material (Fig. S10).

The whole-body motion of the operator is captured with a motion capture suit (Methods), but it cannot be directly used as reference for the robot because of the difference in kinematics (e.g., joint limits, body dimensions) and dynamics (e.g., mass distribution). The system therefore needs to “retarget” the motion [4, 5, 6], that is, to compute references that make sense for the robot. To do so, Cartesian references are scaled using a fixed factor that accounts for the size difference between the human and the operator (Methods). This means that when the operator moves the hands by 10 cm, the robot might move them by only 5cm. The angular references encourage the robot to take the same posture as the operator when it is possible. They are retargeted by mapping each joint of the operator to the robot (Fig. S9) and computing angular positions relative to the initial joint positions. Last, the reference of the center of mass is computed from the human reference to fit the robot kinematics (Methods).

At each time step, given the commands received so far from the operator (for instance, the 3D trajectories of the hands, etc.) the system predicts the most likely future trajectory for the next few seconds (a few hundreds time-steps). The system is trained beforehand on a few example trajectories that encode the different ways of executing a task, using the principle of “motion primitives”: for instance, the human is likely to reach for a bottle on the table with a similar straight hand trajectory

at all times, but the trajectory may be more or less curved in presence of an obstacle. Though human gestures are generally stereotyped, the intrinsic motor noise, the human preference of movement and the small differences in the task executed in the real world (e.g., a displacement of a target object) induce variability in the human motion trajectories to realize a specific task. Even if the trajectory asked by the operator is different from the training set but included in the distributions of what has been previously demonstrated, accurate predictions can still be generated on a short time-scale.

Numerous generic machine learning techniques have been proposed to predict the future of time-series, especially with neural networks [19, 20]. Nevertheless, the robotics community has been working for a long time on regression techniques that are well-suited for robot trajectories. In particular, Movement Primitives (MPs) are a well-established approach for representing and learning motion trajectories in robotics. They provide a data-driven representation of movements and support generalization to novel situations, temporal modulation and sequencing of primitives. Several kinds of MPs have been proposed in the literature. Dynamic Movement Primitives (DMPs) [21] are a formulation of movement primitives with autonomous nonlinear differential equations. The linear parameterization of DMPs makes them suitable for supervised learning from demonstration. Moreover, the temporal, scale, and translation invariance of the differential equations with respect to these parameters provides a useful means for movement recog-

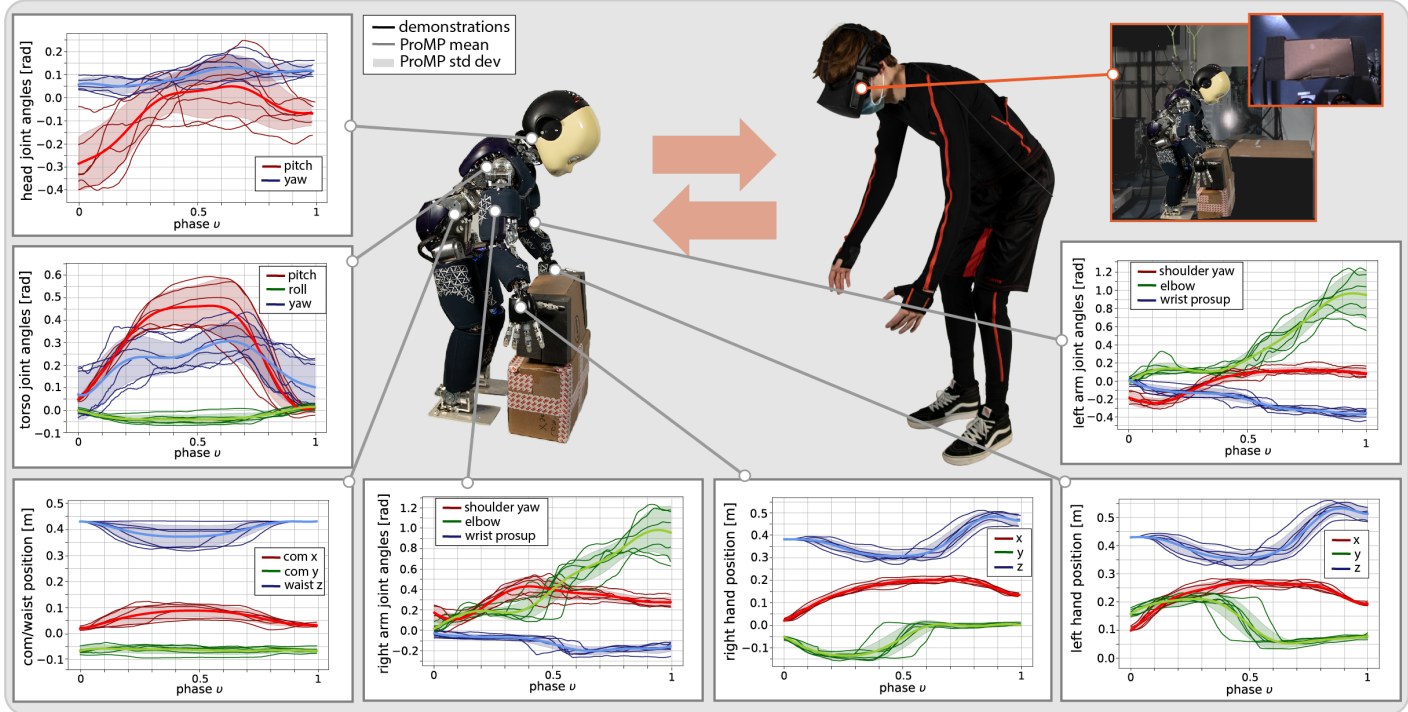


**Fig. 3. Learned predictors for the task of picking up a box at a low position.** For each of the 5 demonstrations, the motion of the operator is first “retargeted” to the robot using the whole-body controller (ignoring delays). The trajectories of each body/joint of the robot is then recorded. From this set of demonstrations (thin lines), a ProMP is fitted for each trajectory; this ProMP is represented here as a thick line (the mean) and a light zone (the standard deviation). The computed mean is a smooth trajectory that averages all the demonstrations and the standard deviation captures the variability of the demonstrations.

nition.

Our system is based on Probabilistic Movement Primitives (ProMPs) [22], which extend the concept of dynamic movement primitives to model the variance of the demonstrations (Methods). Hence, a ProMP is a distribution over trajectories, and an ideal tool to catch the variability of human demonstrations in representing motion primitives [22]. This represents an advantage over deterministic approaches, that can only represent the mean solution. Another advantage of working with distributions is that the properties of motion primitives can be translated into operations from probability theory. For example, modulation of a movement to a novel target can be realized by *conditioning* on the desired target’s positions or partial trajectories [23]. Specifically, our system uses the ProMP’s conditioning operator to adapt the predictions according to observations, hence obtaining an updated prediction for the prosecution of the current movement (Methods).

To evaluate our teleoperation system, we teleoperated the humanoid robot iCub to perform several tasks, for which we found their corresponding motion primitives (Fig. 2), using an inertial motion capture suit and a virtual reality headset (Methods). In the first scenario, the robot had to reach a bottle on a table with the right hand. The bottle could be located in front of the robot or on a box with the two hands, with or without an obstacle in between the robot and the bottle. In the other scenario, the robot had to pick up with the two hands a box, which could be located either on top of another one at different heights or on a table; then it had to place the box either back on the floor, on the table, inside a container or hand it to a person.

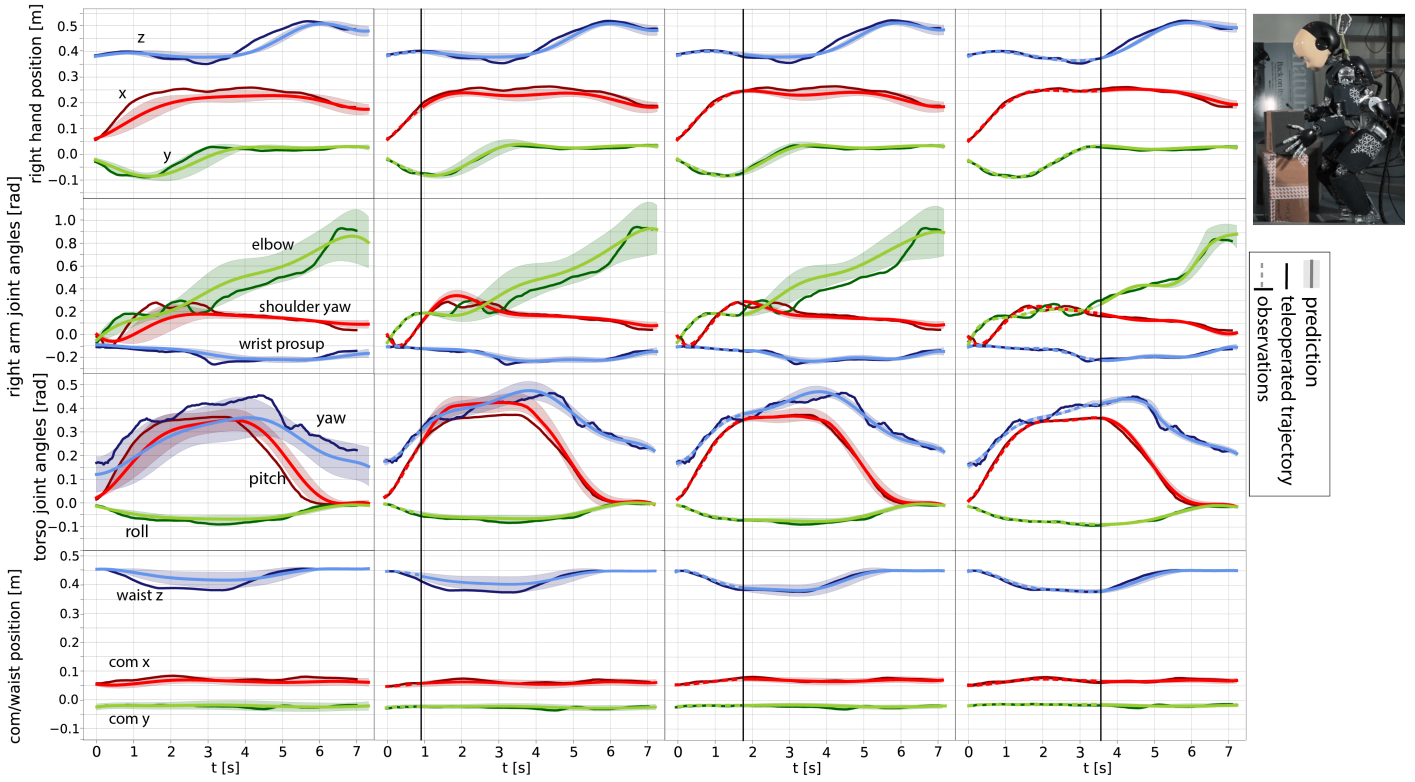
We first teleoperated the robot in a local network, which we consider as an approximation of an ideal network without any delay, to gather a dataset of trajectories. We recorded the trajectories of the center of mass ground projection, the waist height, the hands positions, the arms posture (shoulder rotation, elbow flexion, forearm rotation), the neck posture (flexion and rotation) and the torso posture (flexion, rotation and abduction). For each of these trajectories, a ProMP was learned (Fig. 3, S1). The training set was made of 6 different repetitions of 2 whole-body motions for the bottle reaching scenario (once on the table and once on the box, with an average duration of 5.7 s) and 7 whole-body motions for the box handling scenario (3 for picking up the box, with an average duration of 7.2 s, and 4 for moving the box, with an average duration of 5.8 s), for a total of 54 demonstrations. By comparison with most work in machine learning, this is a small data-set that can be acquired in about 10 minutes with a robot.

We then evaluated the ability of conditioned ProMPs to predict the future motion of the operator, independently of any consideration for teleoperation. At each time-step, the robot identifies which ProMP best

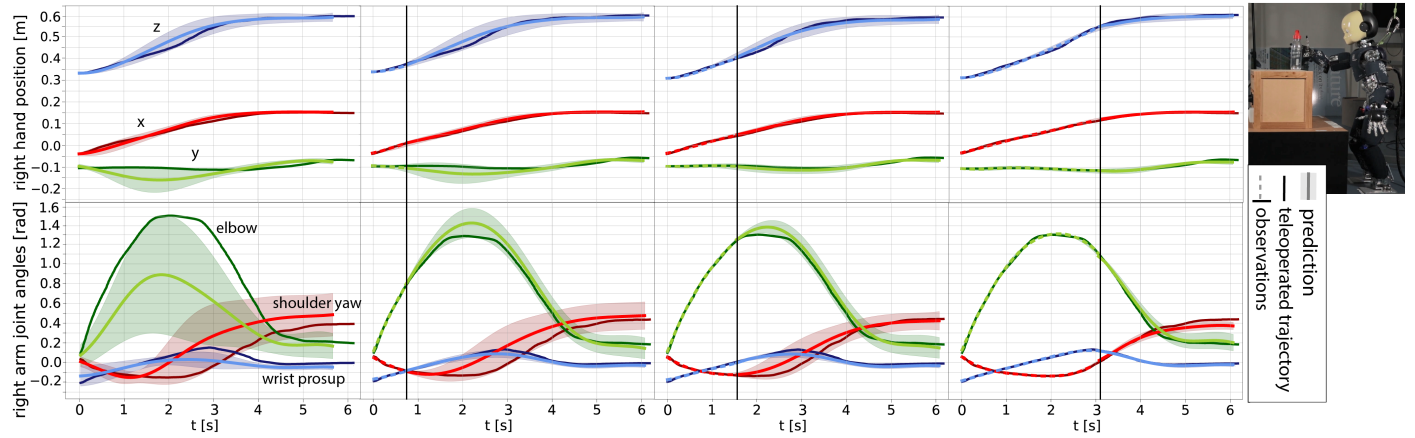
describes the current motion by selecting the ProMP that minimizes the distance between the observations so far and the mean of each ProMP (Methods), and it continuously updates the posterior distribution with the observation. Thanks to the ProMP formulation (Methods), if the best ProMP changes (because of a bad identification or a change of trajectory), the trajectory will transition smoothly to the mean of the right ProMP. Fig. 4 illustrates the quality of the prediction for the two scenarios: after observing a sufficient portion of the trajectory (around 1s) that identifies the ProMP that best describes the current motion, after a fourth of the trajectory, and after half the trajectory. The robot uses the data received so far to predict the trajectory up to the end of the experiment. Visually, the predictions match the actual trajectory very well, although it is smoother, even after less than 1s of observations. In addition, the real trajectory is almost always contained in the distribution of possible trajectories of the prediction (visualized with the variance of the ProMP). To compare quantitatively the prediction to the ground truth, we considered 10 additional whole-body motions not used in the training set and reported in Table 1 the prediction error between the two. The error decreases over time as more observations are available to update the prediction, reaching an error around half centimeter for the Cartesian trajectories after observing half of the motion.

To compensate for the delay, once the robot has identified the best ProMP, it has to select the predictions that correspond to the right time-step from the mean of the ProMP. The time-varying round-trip delay over the communication channel is divided into a forward delay  $\tau_f(t)$  in the data transmission from human to robot, and a backward delay  $\tau_b(t)$  between the robot and the human. Here, we assume that the internal clocks of the robot and the computer of the operators are synchronized to the same world clock reference. As a consequence, the delay  $\tau_f(t)$  can be computed exactly by attaching a time-stamp to the transmitted data and computing the difference between the internal clock and the received time:  $\tau_f(t) = t_{robot} - t_{human}$ . Nevertheless, the delay  $\tau_b(t)$  has to be estimated before being measured because the robot does not know in advance how much time will be required to send the data back to the operator. In this work, we simply assumed it to be equal to the average delay measured in the data transmission ( $\hat{\tau}_b(t) = \bar{\tau}_f$ ).

By computing the round-trip delay, the robot chooses the right samples from the current movement prediction, i.e. posterior ProMPs’ distributions (Fig. 5). At the beginning of the motion, before any ProMP is recognized, the robot uses the delayed commands; however, once a ProMP is recognized, the robot can start compensating for the delays, but first the delayed trajectory needs to catch up with the ProMP. To keep the trajectory smooth, we take inspiration from the shared control literature [24] and use a blending between the current trajectory



(a) The robot is picking up a box in front of it at a mid height.



(b) The robot is reaching a bottle located on top of a box.

**Fig. 4. Prediction update according to observation.** The most relevant predicted trajectories (light colored lines) are compared to the non-delayed trajectories at the operator's side (dark colored lines), after observing different portions of the motion; a perfect prediction would mean that the light line (green/blue/red) line matches the dark line (green/blue/red). This experiment corresponds to a particular experiment reported in Table 1. From left to right, the figure shows the prediction given by the ProMPs learned from the demonstrations, the prediction updated after observing the first portion of motion used to infer the task and its duration, the prediction updated after observing a fourth of the motion, and after observing half of the motion. After less than 1s of observation, the light trajectory is similar to the dark trajectory, whereas it might have been far from the ProMP mean (see, for instance, the elbow in experiment (b)). In most cases, 2 seconds is enough to obtain very accurate predictions for the next 4-5 seconds.

and the mean of the selected ProMP (Methods).

Overall, our *prescient* whole-body teleoperation system relies on the following components:

- a whole-body controller based on quadratic optimization;
- a dataset of whole-body trajectories retargeted from human motions;
- a set of ProMPs that can predict future trajectories given observations;
- a computation of the round-trip delay to select the appropriate commands from the prediction, so that the robot anticipates both the operator-to-robot and the robot-to-operator delays;
- a linear blending to keep the trajectory smooth when there is a large delay, at the start of a trajectory or in case of large delays.

We evaluated the system on the iCub robot with an average round-trip delay of 1.5s (Fig. 6 and Fig. S2.). Additional experiments are presented in Supplementary Materials, in which different tasks are

performed under stochastic round-trip delays ranging from 200ms to 2s (Fig. S3-S6). All the experiments can be seen in Movie 1.

In all our experiments, the operator was able to successfully complete the tasks in spite of these large delays (Fig. 6) thanks to the compensation. Additional experiments show that the robot is not following the mean trajectory from the demonstration, but that it “customizes” the trajectories according to the data received so far (Fig. S8). This means that the operator can perform the task in a specific way and the robot will follow. For example, we can pick up a box by bending the back without using the legs, by bending the legs and limiting back movements, or any other way in between. By continuously updating the ProMPs’ posterior distribution, we can obtain a robot behavior closer to what the human operator is commanding. However, when the delay increases to a significant portion of the complete motion duration, the early delayed observations may not be sufficient to update the posterior distribution of the ProMPs following the actual operator’s commands (especially when the demonstrations exhibit a late variance). In this case (Fig. S7), we obtain a robot behavior that tends to follow the mean of the demonstrations for a significant part of the task. This is visi-

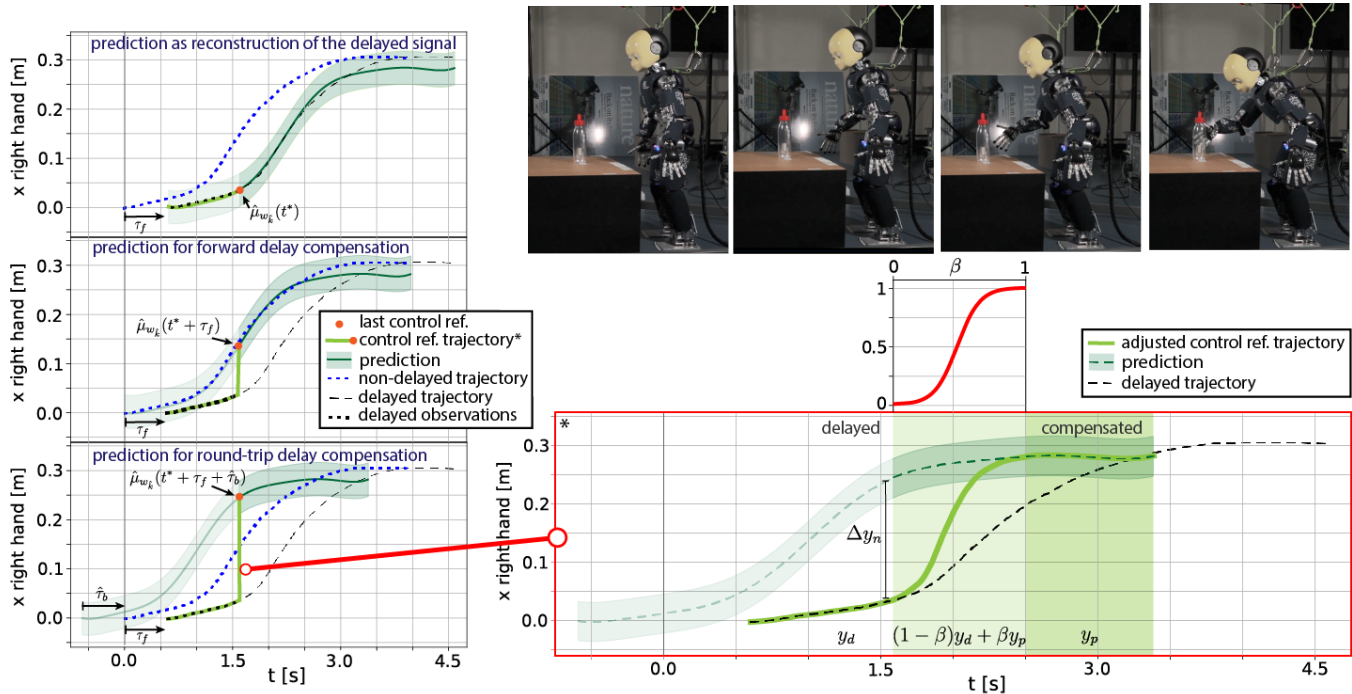


**Fig. 5. Round-trip delay compensation.** By knowing the forward  $\tau_f(t)$  and backward delay  $\tau_b(t)$ , the robot selects the right sample from its prediction of the current command, so as to achieve a synchronization between the operator's movement and the feedback from the robot side. A policy blending arbitrates the delayed observations with the samples selected from the prediction, which guarantees a smooth transition from delayed to compensated teleoperation.

**Table 1. Prediction error after observing different portions of the commanded trajectories.** For 10 whole-body motions not used in the training set, we evaluated the difference between the actual trajectory (commands from the operator) and the predicted trajectory. To understand the influence of the conditioning of the ProMPs, we computed the mean error by following the mean of the ProMP selected by hand ('no obs'), after the initial recognition ('recognition') that takes around 1s, after a fourth of the motion (1/4 motion) and after half of the motion (1/2 motion). Thanks to the conditioning, when more data is used, the prediction is more accurate, which means that the prediction is adjusted to suit the particular motions of the operator (that is, the robot does not simply follow the mean trajectory once it has recognized it). Examples of trajectories are displayed in Fig. 4.

Trajectory	Box handling				Bottle reaching				
	RMS error [rad]				RMS error [rad]				
	no obs	recognition	1/4 motion	1/2 motion		no obs	recognition	1/4 motion	1/2 motion
head yaw	0.102 $\pm$ 0.048	0.079 $\pm$ 0.026	0.043 $\pm$ 0.011	0.011 $\pm$ 0.008	0.080 $\pm$ 0.037	0.039 $\pm$ 0.013	0.023 $\pm$ 0.010	0.010 $\pm$ 0.007	
torso pitch	0.153 $\pm$ 0.062	0.119 $\pm$ 0.045	0.052 $\pm$ 0.029	0.018 $\pm$ 0.008	0.101 $\pm$ 0.051	0.059 $\pm$ 0.020	0.043 $\pm$ 0.011	0.018 $\pm$ 0.008	
torso roll	0.118 $\pm$ 0.048	0.102 $\pm$ 0.037	0.054 $\pm$ 0.028	0.017 $\pm$ 0.008	0.081 $\pm$ 0.042	0.052 $\pm$ 0.015	0.032 $\pm$ 0.010	0.016 $\pm$ 0.008	
torso yaw	0.166 $\pm$ 0.052	0.134 $\pm$ 0.048	0.079 $\pm$ 0.031	0.048 $\pm$ 0.019	0.086 $\pm$ 0.045	0.064 $\pm$ 0.039	0.048 $\pm$ 0.021	0.032 $\pm$ 0.017	
r. should. yaw	0.161 $\pm$ 0.058	0.107 $\pm$ 0.048	0.051 $\pm$ 0.017	0.039 $\pm$ 0.010	0.171 $\pm$ 0.058	0.112 $\pm$ 0.055	0.054 $\pm$ 0.021	0.026 $\pm$ 0.010	
r. elbow	0.167 $\pm$ 0.071	0.144 $\pm$ 0.037	0.096 $\pm$ 0.032	0.032 $\pm$ 0.010	0.219 $\pm$ 0.081	0.095 $\pm$ 0.031	0.064 $\pm$ 0.016	0.033 $\pm$ 0.010	
r. wrist pros.	0.112 $\pm$ 0.049	0.091 $\pm$ 0.022	0.042 $\pm$ 0.012	0.026 $\pm$ 0.008	0.123 $\pm$ 0.052	0.070 $\pm$ 0.021	0.048 $\pm$ 0.016	0.021 $\pm$ 0.008	
	RMS error [cm]					RMS error [cm]			
	no obs	recognition	1/4 motion	1/2 motion		no obs	recognition	1/4 motion	1/2 motion
r. hand x	3.72 $\pm$ 0.89	1.99 $\pm$ 0.47	1.27 $\pm$ 0.39	0.38 $\pm$ 0.11	3.34 $\pm$ 0.78	1.42 $\pm$ 0.57	0.51 $\pm$ 0.31	0.28 $\pm$ 0.14	
r. hand y	3.34 $\pm$ 0.91	1.82 $\pm$ 0.42	0.82 $\pm$ 0.27	0.40 $\pm$ 0.09	3.62 $\pm$ 0.81	1.92 $\pm$ 0.46	0.87 $\pm$ 0.29	0.25 $\pm$ 0.12	
r. hand z	2.69 $\pm$ 0.89	2.24 $\pm$ 0.78	1.02 $\pm$ 0.27	0.46 $\pm$ 0.09	2.57 $\pm$ 0.77	1.92 $\pm$ 0.69	0.65 $\pm$ 0.24	0.20 $\pm$ 0.11	
com x	2.31 $\pm$ 0.66	0.92 $\pm$ 0.23	0.52 $\pm$ 0.20	0.21 $\pm$ 0.12	0.77 $\pm$ 0.52	0.39 $\pm$ 0.21	0.28 $\pm$ 0.12	0.11 $\pm$ 0.09	
com y	1.02 $\pm$ 0.45	0.51 $\pm$ 0.25	0.27 $\pm$ 0.16	0.17 $\pm$ 0.11	0.78 $\pm$ 0.41	0.51 $\pm$ 0.28	0.29 $\pm$ 0.11	0.11 $\pm$ 0.09	
waist z	3.50 $\pm$ 1.01	2.70 $\pm$ 0.91	1.67 $\pm$ 0.56	0.64 $\pm$ 0.22	0.93 $\pm$ 0.35	0.64 $\pm$ 0.21	0.38 $\pm$ 0.19	0.28 $\pm$ 0.13	

ble in Movie 1 as well, where for a round-trip delay around 2s, the robot picked up the box by bending the knees while the human was only using the back without moving the legs.

If, before finishing a given task, the operator decides to stop or to perform another movement, then the predicted trajectories are blended into the delayed trajectories in a way similar to that adopted to switch from delayed to predicted references (Fig. 5), hence avoiding any undesired prolonged mismatch.

To quantify the quality of the compensation, we compared the compensated trajectory to the non-delayed trajectory in 10 different trials which were not used for training, with a stochastic forward delay of  $750\pm300$ ms (Table 2). In the box handling scenario, the results show that the error is less than 1cm for all the considered references (in particular for the hands) whereas without compensation the error is about three times higher (about 3cm for the hands). Similarly, in the bottle reaching task, the error of the compensated trajectory is about 1 to 1.4cm for the hands versus about 4cm for the hands and 1cm for the center of mass when there is no compensation. The angular errors

show a similar pattern. While an error of about 1cm is often enough to achieve a task, for instance grasping an object, an error of 3 to 4 centimeters makes it very likely to miss the object, in addition to be frustrating and disorienting for the operator.

## Discussion

Humanoids could only be deployed at their full potential if they can exploit their whole-body to perform non-trivial, high-value tasks. Whole-body teleoperation is the ideal framework to achieve this goal because it provides an intuitive and flexible approach to operate the robot, provided that the operator can rely on a synchronized feedback. By leveraging machine learning to anticipate the commands of the operator, we showed that it is possible to compensate for delays of 1-2 seconds, which typically correspond to the round-trip communication time between Earth and space [25] and between continents on the Internet [26].

To achieve the synchronization between the human motion and the

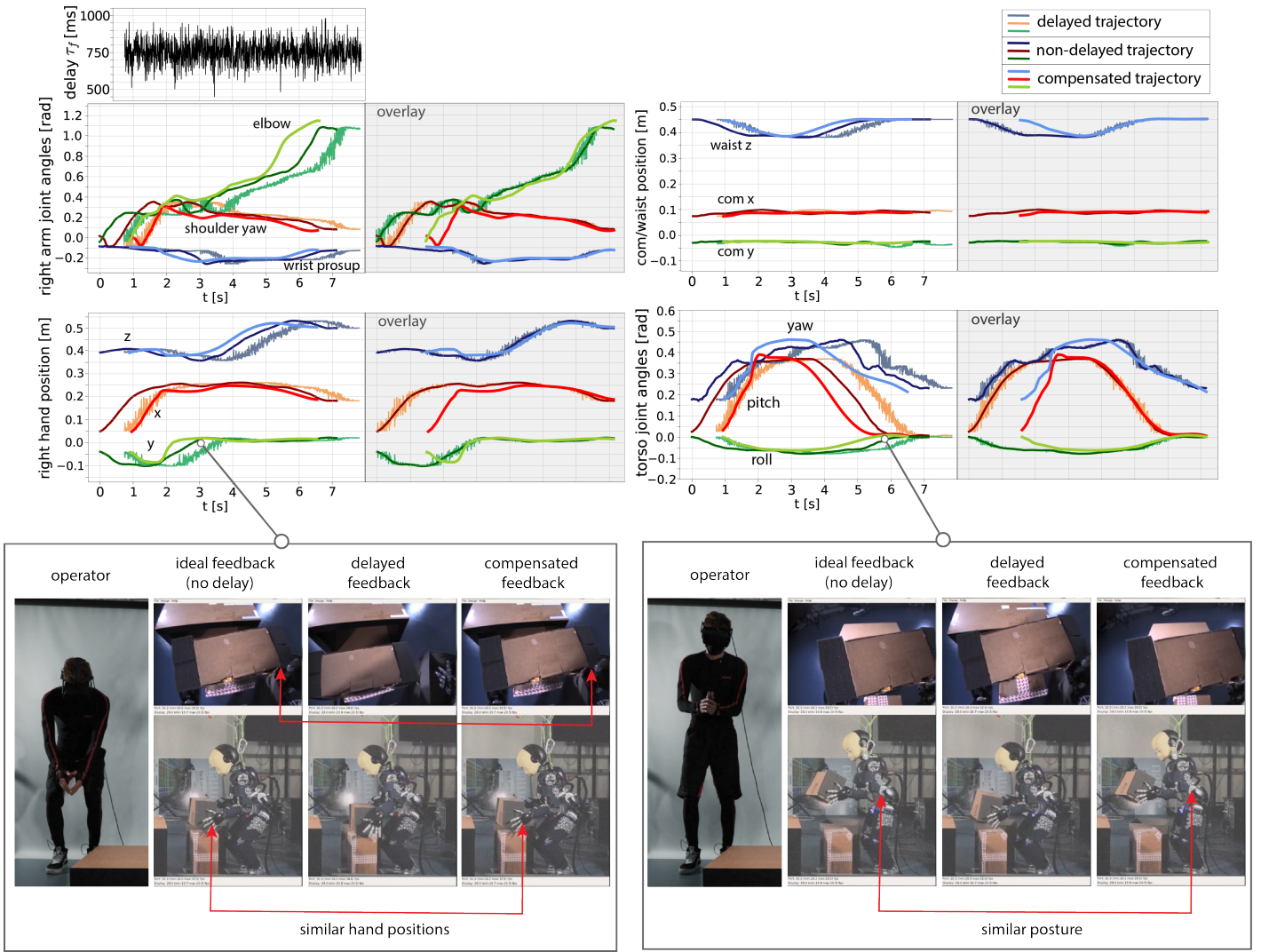


**Fig. 6. Teleoperation with compensation of a round-trip delay around 1.5s.** The robot is picking up a box in front of it at a mid height. The forward delay is around 750ms with a jitter of 300ms. First, the robot reference trajectories follow the delayed teleoperated signals, then when the prediction is available, the robot is able to anticipate the teleoperated motion so to get a visual feedback at the user side coherent with what the operator is doing.

**Table 2. Tracking error between some compensated trajectories and the corresponding non-delayed ones vs compensation error between the non-compensated (delayed) trajectories and the corresponding non-delayed ones.** For comparison purposes, the observation delay is not considered and the compensated trajectories compensate only the forward delay, synchronizing the retargeted human references with the robot control references. The error is computed for 10 different simulated scenarios with a stochastic forward delay of  $750 \pm 300$ ms. Examples of trajectories are displayed in Fig. 6, with the difference of considering no observation delay in the following table.

	Box handling		Bottle reaching		
	RMS error [rad]		RMS error [rad]		
	compensation	no compensation	compensation	no compensation	
head yaw	0.019 $\pm$ 0.008	0.025 $\pm$ 0.008	0.010 $\pm$ 0.004	0.017 $\pm$ 0.009	
torso pitch	0.043 $\pm$ 0.019	0.139 $\pm$ 0.062	0.018 $\pm$ 0.012	0.021 $\pm$ 0.013	
torso roll	0.022 $\pm$ 0.009	0.086 $\pm$ 0.036	0.015 $\pm$ 0.007	0.018 $\pm$ 0.008	
torso yaw	0.067 $\pm$ 0.021	0.124 $\pm$ 0.055	0.015 $\pm$ 0.006	0.020 $\pm$ 0.008	
r. shoulder yaw	0.065 $\pm$ 0.023	0.135 $\pm$ 0.041	0.064 $\pm$ 0.012	0.211 $\pm$ 0.089	
r. elbow	0.063 $\pm$ 0.023	0.198 $\pm$ 0.057	0.194 $\pm$ 0.047	0.394 $\pm$ 0.127	
r. wrist prosup.	0.024 $\pm$ 0.007	0.067 $\pm$ 0.023	0.056 $\pm$ 0.011	0.085 $\pm$ 0.261	
RMS error [cm]					
	compensation	no compensation	compensation	no compensation	
	r. hand x	1.01 $\pm$ 0.34	3.24 $\pm$ 1.28	1.38 $\pm$ 0.37	4.02 $\pm$ 1.76
	r. hand y	0.98 $\pm$ 0.23	3.01 $\pm$ 1.11	1.09 $\pm$ 0.25	2.75 $\pm$ 1.09
	r. hand z	0.96 $\pm$ 0.29	2.91 $\pm$ 0.78	1.05 $\pm$ 0.34	4.91 $\pm$ 1.72
	com x	0.83 $\pm$ 0.11	1.42 $\pm$ 0.46	0.32 $\pm$ 0.07	1.02 $\pm$ 0.24
	com y	0.78 $\pm$ 0.11	1.27 $\pm$ 0.41	0.24 $\pm$ 0.05	1.07 $\pm$ 0.33
	waist z	0.89 $\pm$ 0.13	2.52 $\pm$ 1.34	0.22 $\pm$ 0.07	0.52 $\pm$ 0.08

visual feedback as soon as possible, our approach strongly relies on a fast motion recognition. In fact, if this step required too long, the motion would be over by the time any compensation algorithm could be applied.

In our experiments we leveraged the ProMPs to represent human gesture primitives and also to predict the operator's intention of move-

ment. In the past, we had already used ProMPs with success for real-time prediction of whole-body movements [27] and robot's gestures [28]. They only require few robot/operator demonstrations to be trained, and the posterior update that enables to predict the future trajectory also requires a relatively small set of observations. For the above elements,

they are a suitable and valid technique for predicting the operator's intention in our teleoperation problem. Other data-driven methods for predicting gestures as time-series could be used in principle, for example LSTM-RNN [29, 30], at the expense of more training data and potentially less smooth movements.

As shown in Movie 1 and Fig. 6, we were able to identify the current motion in less than a second, time during which the delayed signals were used to teleoperate the robots. However, our experimental setup included a limited amount of possible tasks (see Fig. 2). If the dataset of possible tasks was larger, the recognition would take a considerable and prohibitive amount of time. In this case, one could resort to other data-driven prediction methods or exploit the fact that human actions are mostly vision guided and identify the object that is about to be manipulated. In such a way, the set of possible tasks would be reduced to those related to that object, accelerating significantly the motion recognition. Yet, this would require the use of object recognition algorithms [31].

The proposed compensation algorithm also relies on the fact that the delay is not comparable to the duration of motion. Indeed, it would not be possible to apply any compensation, if the motion was over before computing any prediction. This is an additional reason for executing the teleoperated tasks at a slow pace (the humanoid robot in our experiments is never teleoperated with fast or rough movements anyway, to avoid damaging the platform).

In addition, the execution speed of a task has to be similar to those recorded during the demonstrations. Once estimated the duration of the current motion, our algorithm does not take into account any duration variation while carrying out the task. A real-time adaptation of the speed execution could be addressed by constantly updating the time modulation of the ProMPs based on the last observations and updating the posterior distribution of the original learned ProMPs based on these observations [27].

Finally, in this study the observation delay is considered to be constant and equal to half the average round-trip delay. However, in real conditions, it could be time varying, generating more jittery videos from the cameras at the robot site. A more accurate estimate of the time varying observation delay should be used in the compensation algorithm so to match the real conditions, as suggested in [32].

The next natural step is to include haptic feedback in addition to visual feedback. First, whole-body feedback would require the operator to wear a full-body exoskeleton [33] or to use less intuitive distributed vibrotactile feedback [34]. In bilateral systems the force signal is directly coupled between robot and human [33], while in master-slave systems the human operator can receive kinesthetic cues not directly related to the contact force being generated by the robot, or as an indirect forces in a passive part of her/his body [34]. Our approach could be certainly extended to the latter case, where ProMPs could be learned for the force signals. The extension to bilateral techniques represents a more complex challenge, since these systems can be very unstable under time-delays. Several approaches have been proposed to stabilize these systems under time delays [35, 36], but the extension to platforms with a high number of degrees of freedom like humanoid robots, and their robustness to packet loss and jittering is still an open challenge.

Visual feedback could be also improved, by using more cameras. In our experiments, we had to use an external camera (in addition to the virtual reality headset) to provide a better situation awareness to the operator about the robot's status in the environment. In fact with the limited field of view of the cameras in the iCub's eyes, the human can hardly see the environment and the robot's body at the same time, which makes it extremely difficult to grasp objects without making any errors. More situation awareness could also be provided to the operator by integrating our method with already existing predictive-display-based techniques [14, 37]: during the non-compensated intervals the predictive display could guide the human operator with a gradual shift from the virtual graphics to the real images of the robot cameras once the synchronization with the user commands has been achieved by our approach. However, the cognitive load of such a solution could be very high and the effects on the performance of the operator and possible impacts on his/her balance should be thoroughly investigated [38].

Overall, this new approach will help deploy more robust, effective, teleoperated systems. It is here demonstrated with a motion capture suit, a virtual reality headset and a state-of-the-art humanoid robot; but this is a general framework that could be used in any other robot, from manipulators to cars, as they could all anticipate remote commands provided that they have a good enough predictor.

## Materials and methods

Our prescient teleoperation system combines six major components (Figure 7): (i) the humanoid robot, (ii) its whole-body controller, (iii) the operator together with the equipment required to control and perceive the robot, (iv) the motion retargeting module, (v) the delayed network and (vi) the delay compensation module.

### The iCub humanoid robot

iCub [15] is a research-grade open-source humanoid robot designed by the Italian Institute of Technology (IIT) to experiment with embodied artificial intelligence. Its height is 104 cm and its weight is 22 kg, which roughly correspond to the proportion of a 5-year old child. iCub has 53 actuated degrees of freedom: 7 in each arm, 9 in each hand (3 for the thumb, 2 for the index, 2 for the middle finger, 1 for the coupled ring and little finger, 1 for the adduction/abduction), 6 in the head (3 for the neck and 3 for the cameras), 3 in the torso/waist, 6 in each leg. In this work, we do not use hands and we do not move the eyes, we therefore control 32 degrees of freedom. The head has stereo cameras in a swivel mounting in the corresponding location of the human eye sockets. iCub is also equipped with six 6-axial force/torque (F/T) sensors in the upper arms, legs and feet, an IMU in the head, and a distributed tactile skin.

### Whole-body controller

The whole-body motion of the robot is defined by the following trajectories: center of mass ground projection, waist height, hands positions, arms postures, neck posture, torso posture; which are either given by the delayed retargeted human motion, or generated by the delay compensation algorithm during the execution of the main task. Each sample of each of these trajectories represents a control reference  $\dot{y}$ . Given  $\dot{y}$ , the robot commands  $q$  are generated by solving the redundant inverse kinematics, which can be formulated as a constrained quadratic programming problem with equality and inequality constraints [17, 5]:

$$\begin{aligned} \arg \min_{\dot{q}} & \sum_i w_i f_i + \sum_j w_j g_j + C\dot{q} \\ f_i &= \|J_i \dot{q} - \dot{x}_i\|^2 \\ g_j &= \|\dot{q}_j - \dot{q}_j^r\|^2 \\ \text{subject to} & \quad J\dot{q} = \dot{x} \\ & A\dot{q} \leq b \end{aligned} \quad (1)$$

The cost function consists of terms  $f_i$  with relative weight  $w_i$  concerning the pose of a specific body link  $i$ , where  $J_i$  is the Jacobian matrix for body link  $i$  and  $\dot{x}_i = \dot{y}_i$  are the reference velocities for body link  $i$ ; and terms  $g_j$  with relative weight  $w_j$  concerning the posture of certain joints  $j$ , where  $\dot{q}_j^r = \dot{y}_j$  are the reference joint velocities for joints  $j$ .  $C\dot{q}$  is a regularization term used to get a unique solution and avoid singularities, where  $C$  is a linear cost vector.

In our implementation, we considered in the terms  $f_i$  the hands positions with  $w_i = 1$  and the waist height with  $w_i = 0.65$ . Instead, the terms  $g_j$  include the head posture with  $w_j = 1$  and the torso posture with  $w_j = 0.72$ , the elbows and wrists posture with  $w_j = 0.11$ . We computed optimal priorities with a multi-objective stochastic optimization that was run in simulation [5]. More details about the whole-body controller can be found in [5].

The equality constraints correspond to the highest priority task, which should be solved exactly. In our implementation, these include the zero moment point position (constrained inside the support polygon) and the feet poses. The inequality constraints contain the robot joint velocity bounds and zero moment point bounds, which is constrained to stay inside the support polygon. The tracking accuracy of the proposed controller is reported in Fig. S10.

Our controller is based on the OpenSOT framework [18] and the qpOASES quadratic programming solver [39].

This controller is run at a frequency of 100 Hz.

### Motion retargeting

The captured human information cannot be directly used as a reference for the humanoid, due to differences in kinematics (e.g. joint limits, body dimensions) and dynamics (e.g. mass distribution) between the human and the robot. Hence, motion retargeting is employed to map the human information into feasible reference trajectories for the robot. For transferring the translational movements of the end-effectors we used a fixed scaling factor (0.4). The joint angles of the human joints instead are manually identified and mapped to the corresponding joints

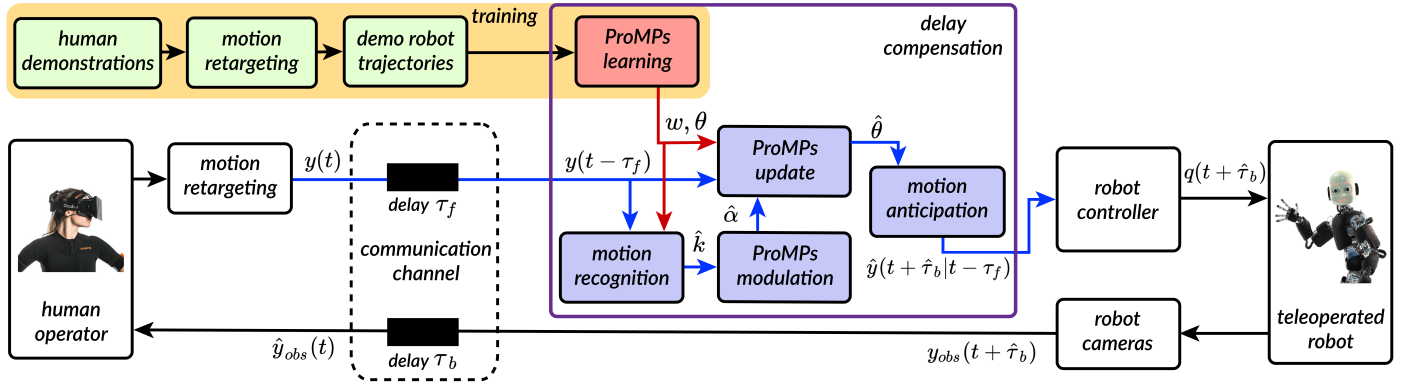


**Fig. 7. Flowchart of the proposed teleoperation system.** During the training phase, the human operator teleoperates the robot without any delay, and performs a variety of tasks. The retargeted human motions represent the robot trajectories demonstrations that are later used to train the ProMPs. A ProMP is learned for every task. When teleoperating the robot in a non-ideal network, the ProMPs are used to predict the robot movement: (1) the system recognizes the current task, that is it identify the most likely ProMP; (2) it estimates the speed of the teleoperated motion and updates the selected ProMPs according to the delayed observed via-points; (3) it compensates for the delay by selecting the trajectory of the posterior ProMPs at the right timestep, so as to synchronize the user movements with what they see from the remote cameras at the robot side. The resulting trajectories are then tracked by the whole-body controller that computes the joint commands for the robot.

of the robot, as shown in Fig. S9. The instantaneous reference value of the robot is then computed as:

$$\Delta q_{iR} = q_{0R} + (q_{iH} - q_{0H}) \quad (2)$$

where  $q$  is the vector of current joint positions,  $\Delta q$  is the vector of joint variations with respect to the initial posture, the indices 0 and  $i$  refer to measurements at initial time and at time  $i$ , and the subindices  $H$  and  $R$  indicate measurements on human and robot, respectively. The same applies for the Cartesian positions of the end-effectors.

For the center of mass, the normalized offset based reconstruction is used [4]. We consider the ground projection of the human center of mass  $p_{com}^g$ . Its position with respect to the left foot is projected onto the line connecting the two feet. The result is then normalized to obtain an offset  $o \in [0, 1]$

$$o = \frac{(\mathbf{p}_{com}^g - \mathbf{p}_{lFoot}^g) \cdot (\mathbf{p}_{rFoot}^g - \mathbf{p}_{lFoot}^g)}{\|\mathbf{p}_{rFoot}^g - \mathbf{p}_{lFoot}^g\|^2}$$

where  $\mathbf{p}_{lFoot}^g$  and  $\mathbf{p}_{rFoot}^g$  are the ground projections of the left and right foot respectively. When the human is in a symmetric pose, the offset  $o$  has a value around 0.5 and when the human stands on a single foot, it is either 0 (left foot) or 1 (right foot). The robot center of mass ground projection is then reconstructed on the line connecting its feet by means of this offset value. To retarget also changes of the center of mass that are not on the line connecting the feet, we can apply the same concept while considering the maximum backward and forward center of mass displacement in the orthogonal direction of the line connecting the feet as done in [4].

## Hardware and communication setup

The human motion is captured by the Xsens MVN system [40], which considers a human model comprising 66 degrees of freedom (corresponding to 22 spherical joints). The user teleoperating the robot is equipped with the wearable motion capture suit MVN Link, consisting of a Lycra suit with 17 inertial measurement units (IMUs) and a wireless data link transmitting at a frequency of 250Hz. Our compensation method receives the delayed data from the motion capture system at 100Hz and transmits to the robot controller at 50Hz.

The user teleoperating the robot is also equipped with a VR Oculus headset. Through the headset, the operator can visualize the delayed images from both an external camera at the robot side, as a third-person view of the teleoperated robot, and the robot cameras, for a first-person view immersive experience.

The communication protocol employed by the network is UDP with a bandwidth of 3Mbps. The delay is artificially generated. The time-varying forward delay  $\tau_f(t)$  is considered as a random variable following a normal distribution with the average forward delay  $\bar{\tau}_f$  as mean, and jitter set to  $\frac{2}{5}\bar{\tau}_f$  and equal to three times the standard deviation<sup>1</sup>. Instead the backward delay  $\tau_b(t)$  is set equal to  $\bar{\tau}_f$ , even if in a real scenario would be time varying, generating more jittery images from the robot cameras. The images from the cameras at the robot side are

<sup>1</sup>Given an observation from a normally distributed random variable  $X$ , with mean  $\mu$  and standard deviation  $\sigma$ , we have  $Pr(\mu - 3\sigma \leq X \leq \mu + 3\sigma) \approx 0.9973$ .

delayed by using the open source application Kinovea [41]. The resulting delayed streaming is projected onto the VR headset through the application Virtual Desktop [42].

## Probabilistic Movement Primitives (ProMPs)

A ProMP [22] is a probabilistic model for representing a trajectory distribution. The movement primitive representation models the time-varying mean and variance of the trajectories and is based on basis-functions. A single trajectory is represented by a weight vector  $\mathbf{w} \in \mathbb{R}^m$ . The probability of observing a trajectory  $\mathbf{y}$  given the underlying weight vector is given as a linear basis function model

$$\xi_t = \Phi_t \mathbf{w} + \epsilon_\xi, \quad (3)$$

$$p(\mathbf{y}|\mathbf{w}) = \prod_t \mathcal{N}(\xi_t | \Phi_t \mathbf{w}, \Sigma_\xi), \quad (4)$$

where  $\Sigma_\xi$  is the observation noise variance,  $\epsilon_\xi \sim \mathcal{N}(0, \Sigma_\xi)$  is the trajectory noise. The matrix  $\Phi_t \in \mathbb{R}^m$  corresponds to the  $m$  normalized radial basis functions evaluated at time  $t$ , with

$$\phi_c(t) = \frac{\exp\left(-\frac{1}{2}(t - \frac{c-1}{m-1})^2\right)}{\sum_{c=1}^m \exp\left(-\frac{1}{2}(t - \frac{c-1}{m-1})^2\right)}, \quad (5)$$

where the variable  $c \in \{1, 2, \dots, m\}$  specifies the center of each basis function. The distribution  $p(\mathbf{w}; \theta)$  over the weight vector  $\mathbf{w}$  is Gaussian, with parameters  $\theta = \{\mu_w, \Sigma_w\}$  specifying the mean and the variance of  $\mathbf{w}$ . The trajectory distribution  $p(\mathbf{y}; \theta)$  is obtained by marginalizing out the weight vector  $\mathbf{w}$ , i.e.

$$p(\mathbf{y}, \theta) = \int p(\mathbf{y}|\mathbf{w})p(\mathbf{w}; \theta)d\mathbf{w}. \quad (6)$$

## Learning ProMPs from demonstrations

The demonstrations are trajectories retargeted from the human. These are recorded in an "offline phase", while the user teleoperates the robot within a local network (approximately without delays) to perform a variety of tasks. Since the duration of each recorded trajectory may be different, a phase variable  $v \in [0, 1]$  is introduced to decouple the movement from the time signal, obtaining a common representation in terms of primitives that is duration independent [27]. For each task, the modulated trajectories  $\xi_i(v)$  are then used to learn a ProMP. The parameters  $\theta = \{\mu_w, \Sigma_w\}$  of the ProMP are estimated by using a simple maximum likelihood estimation algorithm. For each demonstration  $i$ , we compute the weights with linear ridge regression, i.e.

$$\mathbf{w}_i = (\Phi_v^\top \Phi_v + \lambda)^{-1} \Phi_v^\top \xi_i(v), \quad (7)$$

where the ridge factor  $\lambda$  is generally set to a very small value, typically  $\lambda = 10^{-12}$  as in our case, as larger values degrade the estimation of the trajectory distribution. Assuming Normal distributions

$p(\mathbf{w}) \sim \mathcal{N}(\mu_w, \Sigma_w)$ , the mean  $\mu_w$  and covariance  $\Sigma_w$  can be computed from the samples  $\mathbf{w}_i$ :

$$\mu_w = \frac{1}{D} \sum_{i=1}^D \mathbf{w}_i, \quad \Sigma_w = \frac{1}{D} \sum_{i=1}^D (\mathbf{w}_i - \mu_w)(\mathbf{w}_i - \mu_w)^\top, \quad (8)$$

where  $D$  is the number of demonstrations. Since a whole-body trajectory is represented by  $N$  trajectories ( $x$ ,  $y$ ,  $z$  position of the center of mass, of the hands, etc.), we learn a ProMP for each of the  $N$  trajectories. These ProMPs all together encode the same task  $k$ .

## Recognizing the category of motion

Each learned  $k$ -th set of  $N$  ProMPs encodes different whole-body trajectories to accomplish a given task like picking up a box or squatting. To recognize to which set  $k$  the current teleoperated motion belongs to, we can minimize the distance between the first  $n_{obs}$  delayed observations and the mean of the  $N$  ProMPs of a group  $k$ , as done in [27]:

$$\hat{k} = \arg \min_{k \in [1:K]} \left[ \sum_{n=1}^N \sum_{t \in T_{obs}} |\mathbf{y}_n(t - \tau_f(t)) - \Phi_{n,t-\tau_f(t)} \mu_{n,w_k}| \right], \quad (9)$$

where  $K$  is the number of tasks in the dataset and  $T_{obs} = \{t_1, \dots, t_{n_{obs}}\}$  is the set of timesteps associated to the  $n_{obs}$  early observations. While computing  $\hat{k}$ , the ProMPs are modulated to have a duration equal to the mean duration of the demonstrations. The recognition (10) starts whenever a motion is detected, i.e. the derivative of the observed end-effector trajectories exceeds a given threshold. The distance in (10) is continuously computed also after having identified the current motion. In such way, we can verify that the observations do not diverge from the demonstrations (exceed by a given threshold the demonstrated variance), in which case a gradual switch to delayed teleoperation is performed.

## Time-modulation of the ProMPs

During motion recognition, we assumed that the duration of the observed trajectories is equal to the mean duration of the demonstrated trajectories, which might not be true. To match as closely as possible the exact speed at which the movement is being executed by the human operator, we have to estimate the actual trajectory duration (Fig. S8). More specifically, we want to find the time modulation  $\alpha$ , that maps the actual duration of a given (observed) trajectory to the mean duration of the associated demonstrated trajectories.

During the learning step, for each  $k$ -th set of ProMPs we record the set of  $\alpha$  parameters associated to the demonstrations:  $S_{\alpha k} = \{\alpha_1, \dots, \alpha_n\}$ . Then, from this set, we can estimate which  $\alpha$  better fits the current movement speed. We considered as the best  $\hat{\alpha}$  the one that minimizes the difference between the observed trajectory and the predicted trajectory for the first  $n_{obs}$  datapoints:

$$\hat{\alpha} = \arg \min_{\alpha \in S_{\alpha k}} \left\{ \sum_{t \in T_{obs}} |\mathbf{y}(t - \tau_f(t)) - \Phi_{\alpha(t-\tau_f(t))} \mu_{w_k}| \right\}. \quad (10)$$

## Updating the posterior distribution of the ProMPs

Once identified the  $\hat{k}$ -th most likely set of ProMPs and their duration, we continuously update their posterior distribution to take into account the observations that arrive at the robot side. Each ProMP has to be conditioned to reach a certain observed state  $\mathbf{y}_t^*$ . The conditioning for a given observation  $\mathbf{x}_t^* = \{\mathbf{y}_t^*, \Sigma_y^*\}$  (with  $\Sigma_y^*$  being the accuracy of the desired observation), is performed by applying Bayes theorem

$$p(\mathbf{w}_k | \mathbf{x}_t^*) \propto \mathcal{N}(\mathbf{y}_t^* | \Phi_{\hat{\alpha}t} \mathbf{w}_k, \Sigma_y^*) p(\mathbf{w}_k). \quad (11)$$

The conditional distribution of  $p(\mathbf{w}_k | \mathbf{x}_t^*)$  is Gaussian with mean and variance

$$\hat{\mu}_{w_k} = \mu_{w_k} + L(\mathbf{y}_t^* - \Phi_{\hat{\alpha}t}^\top \mu_{w_k}), \quad (12)$$

$$\hat{\Sigma}_{w_k} = \Sigma_{w_k} - L \Phi_{\hat{\alpha}t}^\top \Sigma_{w_k} \Phi_{\hat{\alpha}t}, \quad (13)$$

where

$$L = \Sigma_{w_k} \Phi_{\hat{\alpha}t} (\Sigma_y^* + \Phi_{\hat{\alpha}t}^\top \Sigma_{w_k} \Phi_{\hat{\alpha}t})^{-1}. \quad (14)$$

Given the delay in the transmitted data  $\tau_f(t)$ , we can compute the timestep  $t^*$  at which the ProMP has to be conditioned to a certain observation  $\mathbf{x}_t^*$ :

$$t^* = t - \tau_f(t) - t_0. \quad (15)$$

where  $t_0$  is the starting time of the current motion.

## Motion anticipation

The references for the robot controller are generated at each time based on the updated ProMPs' mean trajectories  $\hat{\mu}_{w_k}$ . For a given ProMP, the sample  $\hat{\mu}_{w_k}(t^*)$  corresponding to the last conditioned observation, is a reconstruction of the past retargeted human input

$$\hat{\mu}_{w_k}(t^*) = \dot{\mathbf{y}}(t - \tau_f(t)). \quad (16)$$

The sample  $\hat{\mu}_w(t^* + \tau_f(t))$  is an estimate of the current retargeted human input

$$\hat{\mu}_{w_k}(t^* + \tau_f(t)) = \hat{\mathbf{y}}(t), \quad (17)$$

and could be used to synchronize the human movement with that of the robot, compensating only the forward delay (see Fig. 7). In our case, we want to synchronize the motion of the human operator with what is seen from the robot side, hence compensating both the forward and backward delays. To do so, we select as a control reference the sample  $\hat{\mu}_w(t^* + \tau_f(t) + \hat{\tau}_b(t))$ , which corresponds to a future prediction of the retargeted human movements:

$$\hat{\mu}_{w_k}(t^* + \tau_f(t) + \hat{\tau}_b(t)) = \hat{\mathbf{y}}(t + \hat{\tau}_b(t)). \quad (18)$$

Also the remaining samples  $[\hat{\mu}_{w_k}(t^* + \tau_f(t) + \hat{\tau}_b(t) + 1), \hat{\mu}_{w_k}(t^* + \tau_f(t) + \hat{\tau}_b(t) + 2), \dots]$  are given to the controller. They are used as control reference if a new reference cannot be computed in the next control step due to packet losses or jitter.

After generating a first prediction, the transition from delayed to predicted references can be discontinuous (Figure 5). To smoothen the transition, a policy blending arbitrates the delayed received references  $\mathbf{y}(t - \tau_f(t))$  and the predicted ones  $\hat{\mathbf{y}}(t + \hat{\tau}_b(t) | t - \tau_f(t))$ , determining the adjusted reference (Fig. 5):

$$\hat{\mathbf{y}}'(t + \hat{\tau}_b(t) | t - \tau_f) = (1 - \beta) \mathbf{y}_d + \beta \mathbf{y}_p, \quad (19)$$

where  $\mathbf{y}_d = \mathbf{y}(t - \tau_f(t))$ ,  $\mathbf{y}_p = \hat{\mathbf{y}}(t + \hat{\tau}_b(t) | t - \tau_f(t))$ ,  $\beta = \{\beta_0, \dots, \beta_n, \dots, \beta_N\}^\top$  with  $\beta_n \in [0, 1]$

$$\beta_n = \frac{1}{1 + e^{-12(\frac{i}{\Delta y_n} - \frac{1}{2})}}, \quad (20)$$

$i = \{0, 1, \dots, \Delta y_n\}$  and  $\Delta y_n$  is the initial difference between a delayed reference and the corresponding prediction expressed in mm (for Cartesian trajectories) or deg  $\times 10^{-1}$  (for postural trajectories).

## Supplementary Materials

- Fig. S1. Learned ProMPs for the task of reaching a bottle on the table.
- Fig. S2. Reaching a bottle with compensation of a round-trip delay around 1.5s.
- Fig. S3. Teleoperation with compensation of a round-trip delay around 200ms.
- Fig. S4. Teleoperation with compensation of a round-trip delay around 500ms.
- Fig. S5. Teleoperation with compensation of a round-trip delay around 1s.
- Fig. S6. Teleoperation with compensation of a round-trip delay around 2s.
- Fig. S7. Tracking error between the compensated trajectories and those non-delayed for a round-trip delay around 1.5s.
- Fig. S8. Teleoperation with a round-trip delay around 1.5s compensated by our approach vs learned trajectories distributions.
- Fig. S9. Teleoperation with a round-trip delay around 2s compensated by our approach vs learned trajectories distributions.
- Fig. S10. Time modulation estimation.
- Fig. S11. Posture retargeting from human (Xsens system) to iCub.
- Fig. S12. Teleoperation controller tracking error.

## Acknowledgements

The authors would like to thank E. Ghini for the precious help and support provided during the experiments.

**Funding:** This work was supported by the European Union Horizon 2020 Research and Innovation Program under Grant Agreement No. 731540 (project AnDy), by the European Research Council (ERC) under Grant Agreement No. 637972 (project ResiBots), an Inria-DGA grant (“humanoïde résilient”), and the Inria “ADT” wbCub/wbTorque. Experiments were performed in the Creativ’Lab facilities, supported by the FEDER Sciarat.

**Author contributions:** L.P. implemented the system and performed the experiments. J.-B.M. and S.I. proposed the initial concept and supervised the study. L.P., J.-B.M. and S.I. analyzed the results and wrote the article.

**Competing interests:** The authors declare that they have no competing financial interests.

**Data and materials availability:** All data needed to evaluate the conclusions in the paper are present in the paper, the Supplementary Materials and in <https://zenodo.org/record/4906336> (dataset of off-line training and on-line testing control reference trajectories).

## References

- [1] K. Yamane and A. Murai, *A Comparative Study Between Humans and Humanoid Robots*. Dordrecht: Springer Netherlands, 2016, pp. 1–20. [Online]. Available: [https://doi.org/10.1007/978-94-007-7194-9\\_7-1](https://doi.org/10.1007/978-94-007-7194-9_7-1)
- [2] C. Atkeson, B. P. Wisely Babu, N. Banerjee, D. Berenson, C. Bove, X. Cui, M. Dedonato, R. Du, S. Feng, P. Franklin, M. Gennert, J. Graff, P. He, A. Jaeger, J. Kim, K. Knoedler, L. Li, C. Liu, X. Long, and X. Xinjilefu, *What Happened at the DARPA Robotics Challenge Finals*, 2018, pp. 667–684.
- [3] M. Stilman, K. Nishiwaki, and S. Kagami, “Humanoid teleoperation for whole body manipulation,” in *2008 IEEE International Conference on Robotics and Automation*. IEEE, 2008, pp. 3175–3180.
- [4] L. Penco, B. E. P. Clement, V. Modugno, E. M. Hoffman, G. Nava, D. Pucci, N. G. Tsagarakis, J.-B. Mouret, and S. Ivaldi, “Robust real-time whole-body motion retargeting from human to humanoid,” *2018 IEEE-RAS 18th International Conference on Humanoid Robots (Humanoids)*, pp. 425–432, 2018.
- [5] L. Penco, E. M. Hoffman, V. Modugno, W. Gomes, J. Mouret, and S. Ivaldi, “Learning robust task priorities and gains for control of redundant robots,” *IEEE Robotics and Automation Letters*, vol. 5, no. 2, pp. 2626–2633, 2020.
- [6] L. Penco, N. Scianca, V. Modugno, L. Lanari, G. Oriolo, and S. Ivaldi, “A multi-mode teleoperation framework for humanoid loco-manipulation: An application for the iCub robot,” *IEEE Robotics Automation Magazine*, vol. 26, no. 4, pp. 73–82, 2019.
- [7] W. R. Ferrell, “Remote manipulation with transmission delay,” *IEEE Transactions on Human Factors in Electronics*, vol. HFE-6, no. 1, pp. 24–32, 1965.
- [8] W. R. Ferrell and T. B. Sheridan, “Supervisory control of remote manipulation,” *IEEE Spectrum*, vol. 4, no. 10, pp. 81–88, 1967.
- [9] National Aeronautics and Space Administration (NASA)-Centennial Challenges Program-Space Robotics Challenge Phase 2. [Online]. Available: [https://www.fbo.gov/index?s=opportunity&mode=form&id=6b4c9a474d2edd9934be7008edc665cd&tab=core&\\_cview=0](https://www.fbo.gov/index?s=opportunity&mode=form&id=6b4c9a474d2edd9934be7008edc665cd&tab=core&_cview=0). [Accessed: 1-May-2020]
- [10] N. Lii, C. Riecke, D. Leidner, S. Schätzle, P. Schmaus, B. Weber, T. Krueger, M. Stelzer, A. Wedler, and G. Grunwald, “The robot as an avatar or co-worker? an investigation of the different teleoperation modalities through the kontur-2 and meteron supvis justin space telerobotic missions,” in *69th International Astronautical Congress (IAC)*, 2018.
- [11] L. Peñin, K. Matsumoto, and K. U. G. Kenkyūjo, *Teleoperation with Time Delay: A Survey and Its Use in Space Robotics*. National Aerospace Laboratory, 2002. [Online]. Available: <https://books.google.fr/books?id=NhzGwAACAAJ>
- [12] M. Hernando and E. Gamboa, *Teleprogramming: Capturing the Intention of the Human Operator*. Berlin, Heidelberg: Springer Berlin Heidelberg, 2007, pp. 303–320.
- [13] A. K. Bejczy, W. S. Kim, and S. C. Venema, “The phantom robot: predictive displays for teleoperation with time delay,” in *Proceedings., IEEE International Conference on Robotics and Automation*, 1990, pp. 546–551 vol.1.
- [14] P. Mitra and G. Niemeyer, “Mediating time delayed teleoperation with user suggested models: Implications and comparative study,” in *2008 Symposium on Haptic Interfaces for Virtual Environment and Teleoperator Systems*, 2008, pp. 343–350.
- [15] L. Natale, C. Bartolozzi, D. Pucci, A. Wykowska, and G. Metta, “iCub: The not-yet-finished story of building a robot child,” *Science Robotics*, vol. 2, no. 13, 2017.
- [16] G. Metta, L. Natale, F. Nori, G. Sandini, D. Vernon, L. Fadiga, C. von Hofsten, K. Rosander, M. Lopes, J. Santos-Victor, A. Bernardino, and L. Montesano, “The iCub humanoid robot: An open-systems platform for research in cognitive development,” *Neural Networks*, vol. 23, no. 8, pp. 1125–1134, 2010, social Cognition: From Babies to Robots.
- [17] A. Escande, N. Mansard, and P.-B. Wieber, “Hierarchical quadratic programming: Fast online humanoid-robot motion generation,” *The International Journal of Robotics Research*, vol. 33, no. 7, pp. 1006–1028, 2014.
- [18] A. Rocchi, E. M. Hoffman, D. G. Caldwell, and N. G. Tsagarakis, “Opensot: a whole-body control library for the compliant humanoid robot coman,” in *2015 IEEE International Conference on Robotics and Automation (ICRA)*. IEEE, 2015, pp. 6248–6253.
- [19] A. R. S. Parmezan, V. M. Souza, and G. E. Batista, “Evaluation of statistical and machine learning models for time series prediction: Identifying the state-of-the-art and the best conditions for the use of each model,” *Information sciences*, vol. 484, pp. 302–337, 2019.
- [20] B. Lim and S. Zohren, “Time series forecasting with deep learning: A survey,” *Philosophical Transactions of the Royal Society: A*, p. 3792020020920200209, 2021.
- [21] S. Schaal, *Dynamic Movement Primitives -A Framework for Motor Control in Humans and Humanoid Robotics*. Tokyo: Springer Tokyo, 2006, pp. 261–280. [Online]. Available: [https://doi.org/10.1007/4-431-31381-8\\_23](https://doi.org/10.1007/4-431-31381-8_23)
- [22] A. Paraschos, C. Daniel, J. Peters, and G. Neumann, “Using probabilistic movement primitives in robotics,” *Autonomous Robots*, vol. 42, 07 2017.
- [23] G. J. Maeda, G. Neumann, M. Ewerton, R. Lioutikov, O. Kroemer, and J. Peters, “Probabilistic movement primitives for coordination of multiple human–robot collaborative tasks,” *Autonomous Robots*, vol. 41, no. 3, pp. 593–612, 2017.
- [24] D. P. Losey, C. G. McDonald, E. Battaglia, and M. K. O’Malley, “A Review of Intent Detection, Arbitration, and Communication Aspects of Shared Control for Physical Human–Robot Interaction,” *Appl. Mech. Rev.*, vol. 70, no. 1, 02 2018.
- [25] N. Y. Lii, D. Leidner, A. Schiele, P. Birkenkampf, B. Pleintinger, and R. Bayer, “Command robots from orbit with supervised autonomy: An introduction to the meteron supvis-justin experiment,” in *Proceedings of the Tenth Annual ACM/IEEE International Conference on Human-Robot Interaction Extended Abstracts*, ser. HRI’15 Extended Abstracts. New York, NY, USA: Association for Computing Machinery, 2015, p. 53–54. [Online]. Available: <https://doi.org/10.1145/2701973.2702022>
- [26] T. Holand-Jørgensen, B. Ahlgren, P. Hurtig, and A. Brunstrom, “Measuring latency variation in the internet,” in *Proceedings of the 12th International Conference on emerging Networking EXperiments and Technologies*, 2016, pp. 473–480.
- [27] O. Dermy, A. Paraschos, M. Ewerton, J. Peters, F. Charpillet, and S. Ivaldi, “Prediction of intention during interaction with icub with probabilistic movement primitives,” *Frontiers in Robotics and AI*, vol. 4, p. 45, 2017.
- [28] O. Dermy, M. Chaveroche, F. Colas, F. Charpillet, and S. Ivaldi, “Prediction of human whole-body movements with ae-prompts,” in *2018 IEEE-RAS 18th International Conference on Humanoid Robots (Humanoids)*. IEEE, 2018, pp. 572–579.
- [29] X. Zhao, S. Chumkamon, S. Duan, J. Rojas, and J. Pan, “Collaborative human–robot motion generation using lstm-rnn,” in *2018 IEEE-RAS 18th International Conference on Humanoid Robots (Humanoids)*, 2018, pp. 1–9.
- [30] M. Anvaripour, M. Khoshnam, C. Menon, and M. Saif, “Fmg- and rnn-based estimation of motor intention of upper-limb motion in human–robot collaboration,” *Frontiers in Robotics and AI*, vol. 7, p. 183, 2020. [Online]. Available: <https://www.frontiersin.org/article/10.3389/frobt.2020.573096>
- [31] M. Tan, R. Pang, and Q. V. Le, “Efficientdet: Scalable and efficient object detection,” in *Proceedings of the IEEE/CVF Conference on Computer Vision and Pattern Recognition (CVPR)*, June 2020.
- [32] O. Gurewitz, I. Cidon, and M. Sidi, “One-way delay estimation using network-wide measurements,” *IEEE Transactions on Information Theory*, vol. 52, no. 6, pp. 2710–2724, 2006.
- [33] J. Ramos and S. Kim, “Dynamic locomotion synchronization of bipedal robot and human operator via bilateral feedback teleoperation,” *Science Robotics*, vol. 4, no. 35, 2019.
- [34] A. Brygo, I. Sarakoglou, N. Garcia-Hernandez, and N. Tsagarakis, “Humanoid robot teleoperation with vibrotactile based balancing feedback,” in *Int. Conf. on Human Haptic Sensing and Touch Enabled Computer Applications*, Jun 2014.
- [35] X. Xu and E. Steinbach, “Elimination of cross-dimensional artifacts in the multi-dof time domain passivity approach for time-delayed teleoperation with haptic feedback,” in *2019 IEEE World Haptics Conference (WHC)*, doi: 10.1109/WHC.2019.8816074, 2019.
- [36] H. Singh, M. Panzirsch, A. Coelho, and C. Ott, “Proxy-based approach for position synchronization of delayed robot coupling without sacrificing performance,” *IEEE Robotics and Automation Letters*, vol. 5, no. 4, pp. 6599–6606, 2020.
- [37] D. Valenzuela-Urrutia, R. Muñoz-Riffo, and J. R. del Solar, “Virtual reality-based time-delayed haptic teleoperation using point cloud data,” *Journal of Intelligent & Robotic Systems*, pp. 1–14, 2019.
- [38] H. Hu, C. Perez, H.-X. Sun, and M. Jagersand, “Performance of predictive display teleoperation under different delays with different degree of freedoms,” in *2016 International Conference on Information System and Artificial Intelligence (ISAI)*, 2016, pp. 380–384.
- [39] H. J. Ferreau, C. Kirches, A. Potschka, H. G. Bock, and M. Diehl, “qpoases: A parametric active-set algorithm for quadratic programming,” *Mathematical Programming Computation*, vol. 6, no. 4, pp. 327–363, 2014.

- [40] D. Roetenberg, H. Luinge, and P. Slycke, "Xsens mvn: Full 6dof human motion tracking using miniature inertial sensors," *Xsens Motion Technol. BV Tech. Rep.*, vol. 3, 01 2009.
- [41] Kinovea. A microscope for your videos. [Online]. Available: <https://www.kinovea.org/>
- [42] Virtual Desktop. Your PC in VR. [Online]. Available: <https://www.vrdesktop.net/>

# Supplementary material

# Prescient teleoperation of humanoid robots

Luigi Penco<sup>1</sup>, Jean-Baptiste Mouret<sup>1</sup>, Serena Ivaldi<sup>1</sup>

<sup>1</sup> Inria Nancy – Grand Est, CNRS, Université de Lorraine, France

serena.ivaldi@inria.fr

- Movie M1: <https://youtu.be/N3u4ot3aIyQ>
- Fig. S1. Learned ProMPs for the task of reaching a bottle on the table.
- Fig. S2. Reaching a bottle with compensation of a round-trip delay around 1.5s.
- Fig. S3. Teleoperation with compensation of a round-trip delay around 200ms.
- Fig. S4. Teleoperation with compensation of a round-trip delay around 500ms.
- Fig. S5. Teleoperation with compensation of a round-trip delay around 1s.
- Fig. S6. Teleoperation with compensation of a round-trip delay around 2s.
- Fig. S7. Tracking error between the compensated trajectories and those non-delayed for a round-trip delay around 1.5s.
- Fig. S8. Teleoperation with a round-trip delay around 1.5s compensated by our approach vs learned trajectories distributions.
- Fig. S9. Teleoperation with a round-trip delay around 2s compensated by our approach vs learned trajectories distributions.
- Fig. S10. Time modulation estimation.
- Fig. S11. Posture retargeting from human (Xsens system) to iCub.
- Fig. S12. Teleoperation controller tracking error.

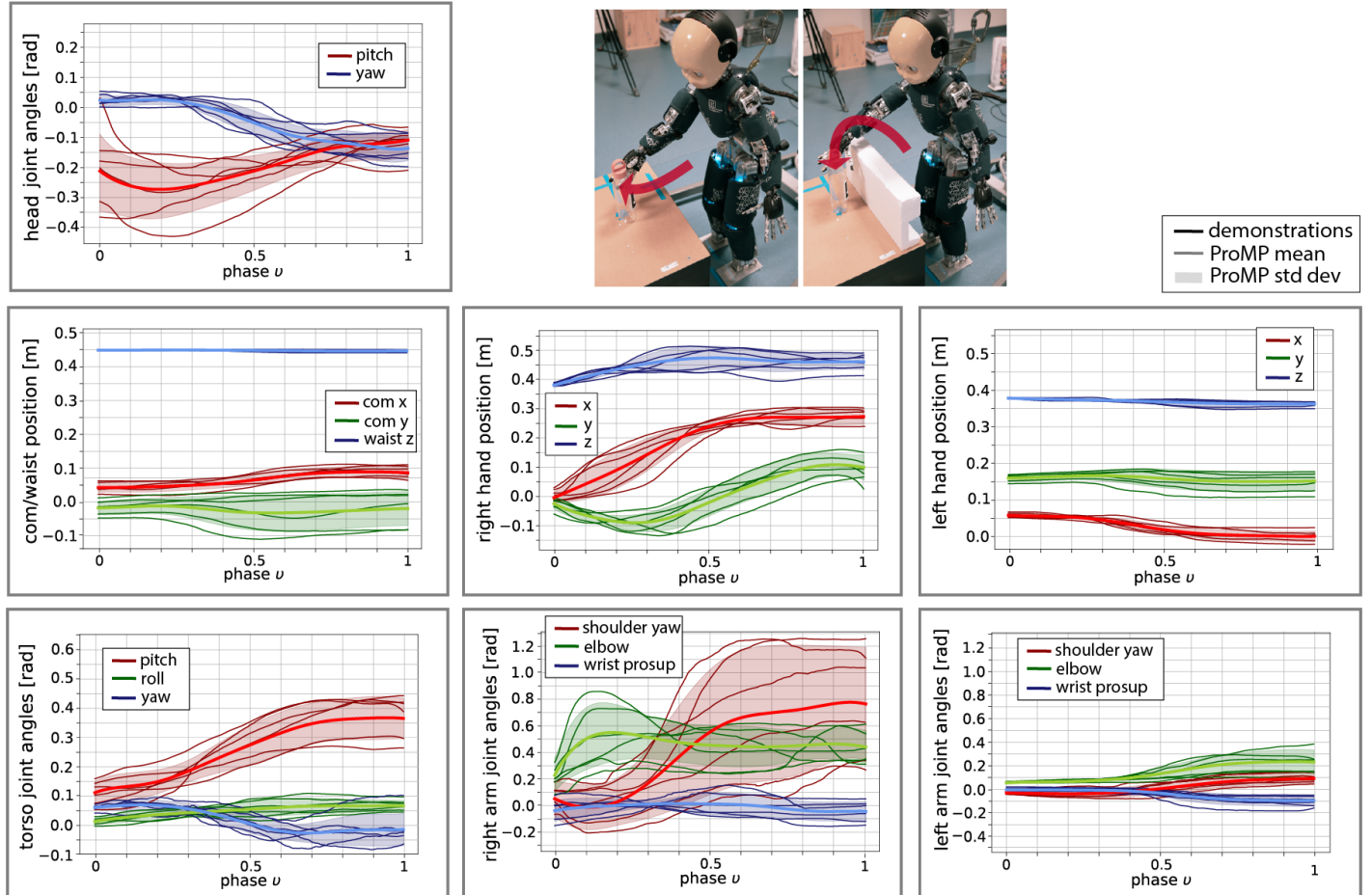


**Fig. S1. Learned ProMPs for the task of reaching a bottle on the table.** The whole-body motion of the teleoperated robot is obtained by following the reference trajectories retargeted from the human. We learned a ProMP for each of these trajectories, given 6 demonstrations in a local network without any delay.

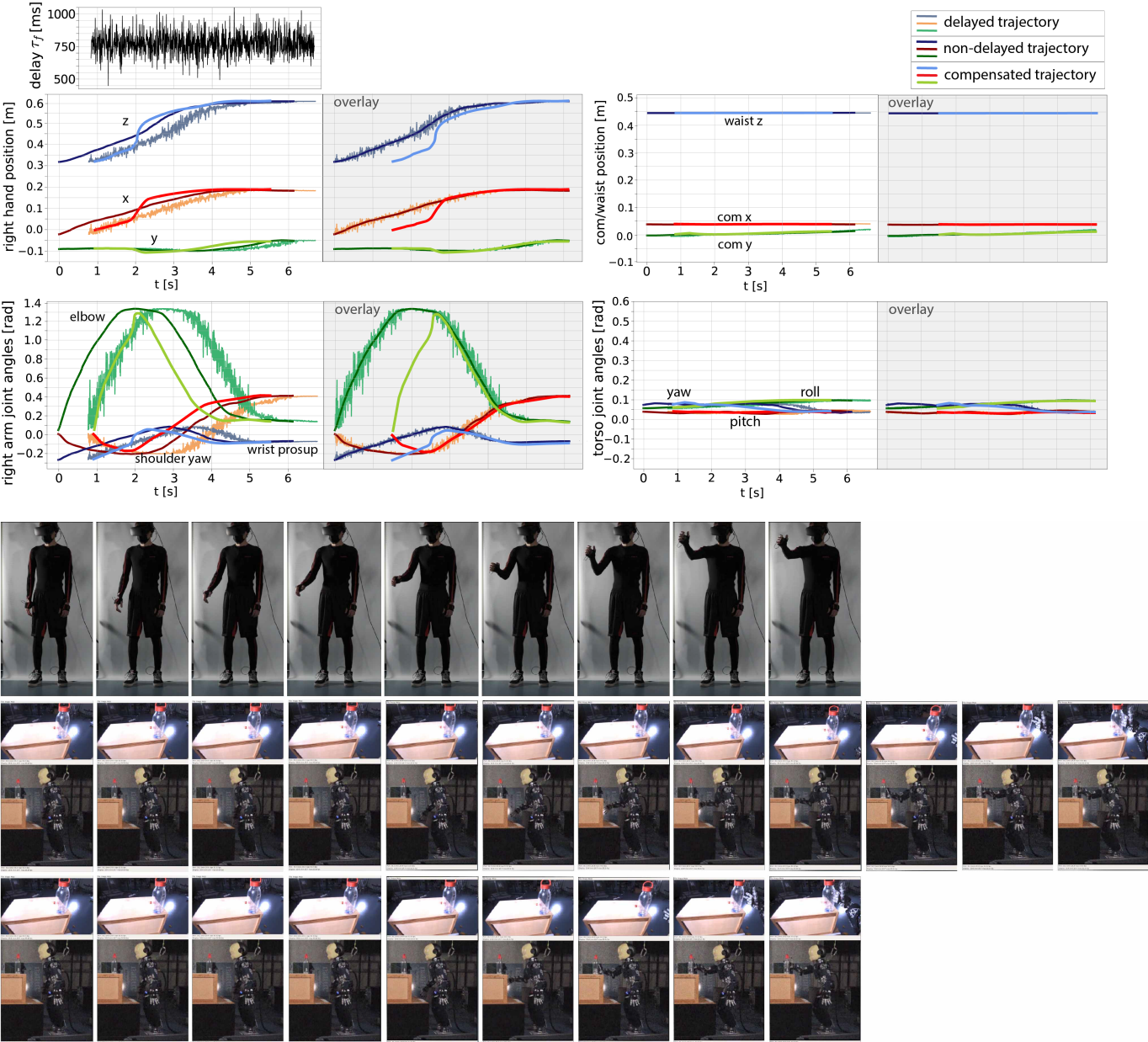


**Fig. S2. Reaching a bottle with compensation of a round-trip delay around 1.5s.** The robot is reaching a bottle located on top of a box. The forward delay is around 750ms with a jitter of 300ms. First, the robot reference trajectories follow the delayed teleoperated signals, then when the prediction is available, the robot is able to anticipate the teleoperated motion so to get a visual feedback at the user side coherent with what the operator is doing.

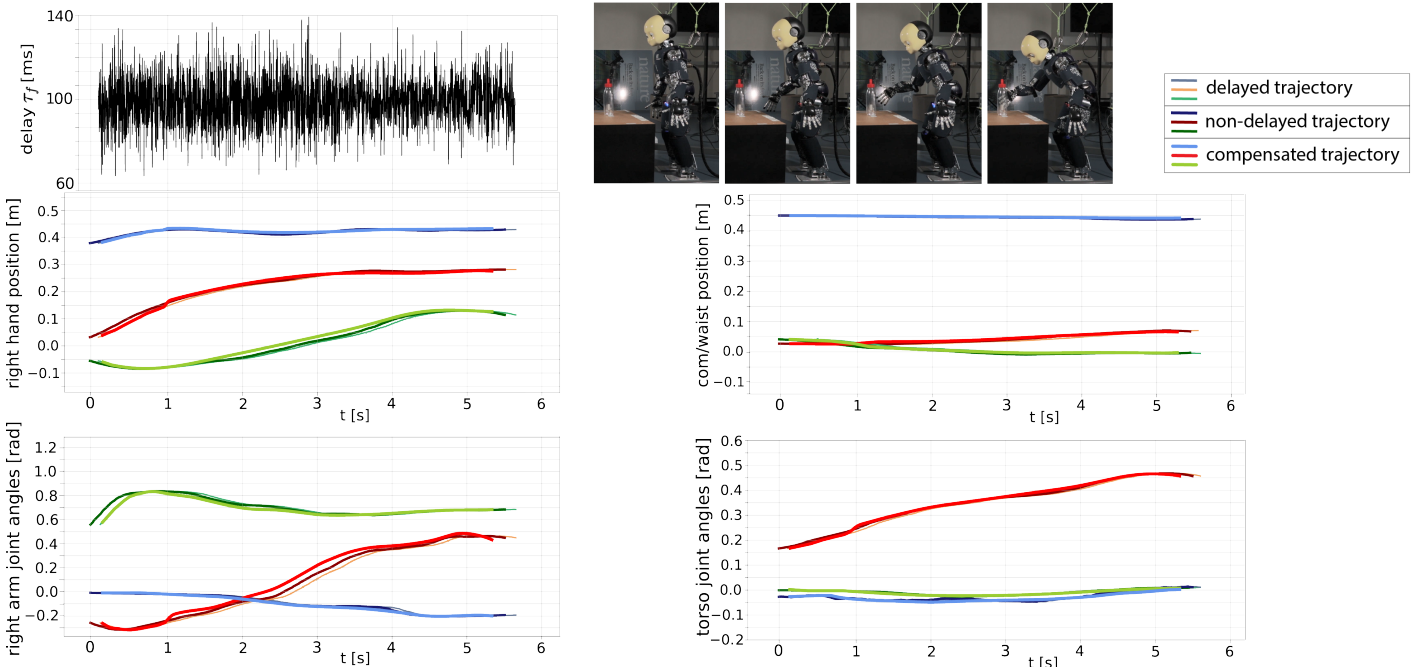
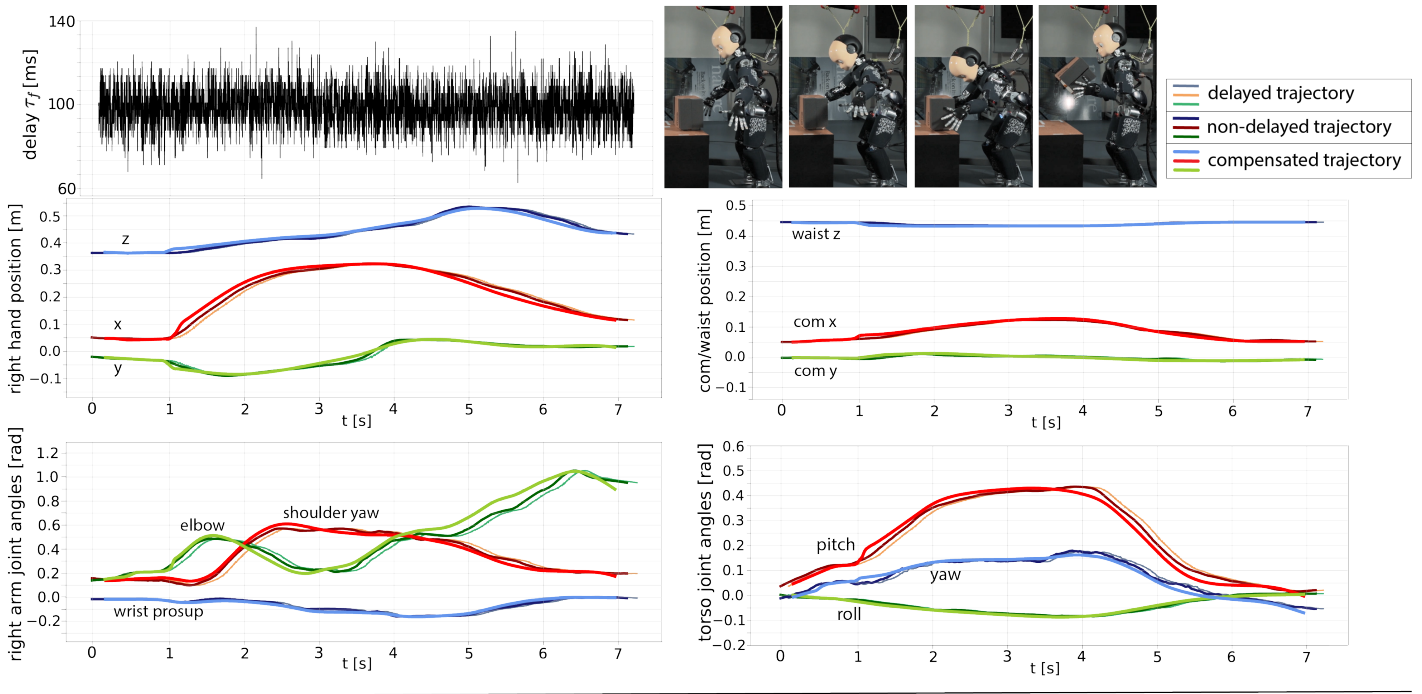


**Fig. S3. Teleoperation with compensation of a round-trip delay around 200ms.** Top: The robot is picking up a box located on a table. Bottom: The robot is reaching a bottle located on a table. The forward delay is around 100ms with a jitter of 40ms. First, the robot reference trajectories follow the delayed teleoperated signals, then when the prediction is available, the robot is able to anticipate the teleoperated motion.

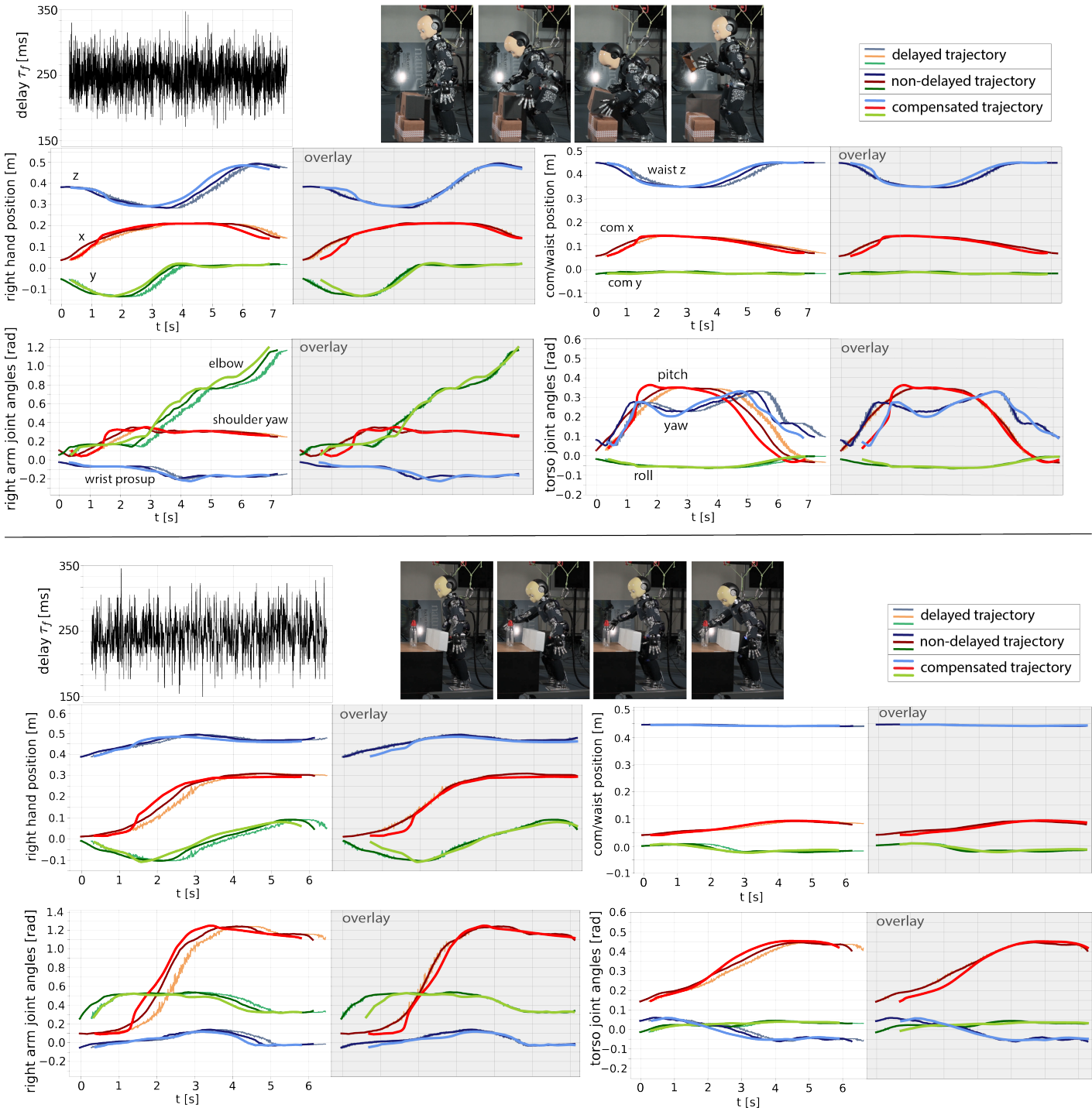


**Fig. S4. Teleoperation with compensation of a round-trip delay around 500ms.** Top: The robot is picking up a box in front of it at a low height. Bottom: The robot is reaching a bottle located on the table behind an obstacle. The forward delay is around 250ms with a jitter of 100ms. First, the robot reference trajectories follow the delayed teleoperated signals, then when the prediction is available, the robot is able to anticipate the teleoperated motion.

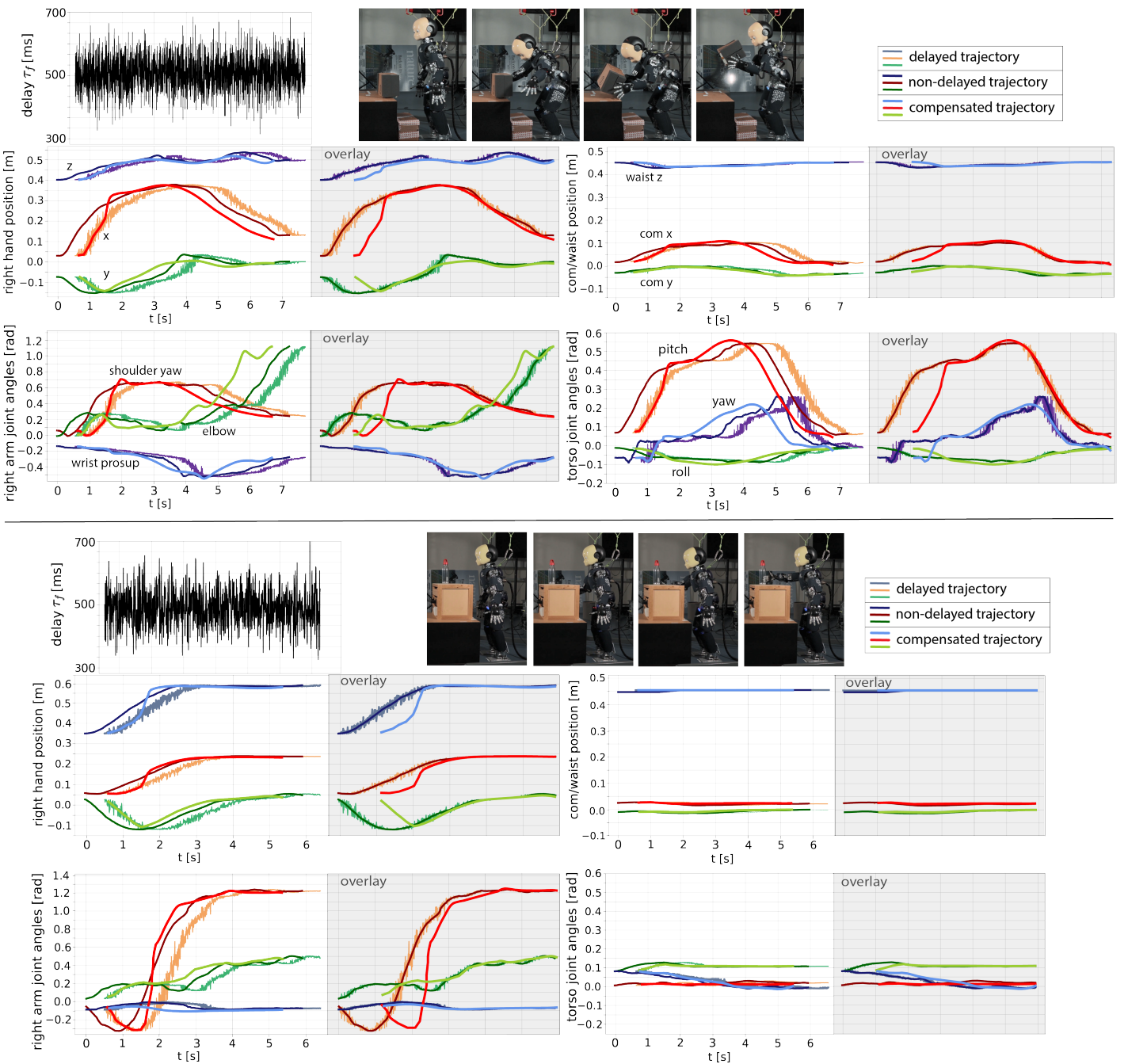


**Fig. S5. Teleoperation with compensation of a round-trip delay around 1s.** Top: The robot is picking up a box located on a table. Bottom: The robot is reaching a bottle located on a box, on the table. The forward delay is around 500ms with a jitter of 200ms. First, the robot reference trajectories follow the delayed teleoperated signals, then when the prediction is available, the robot is able to anticipate the teleoperated motion.

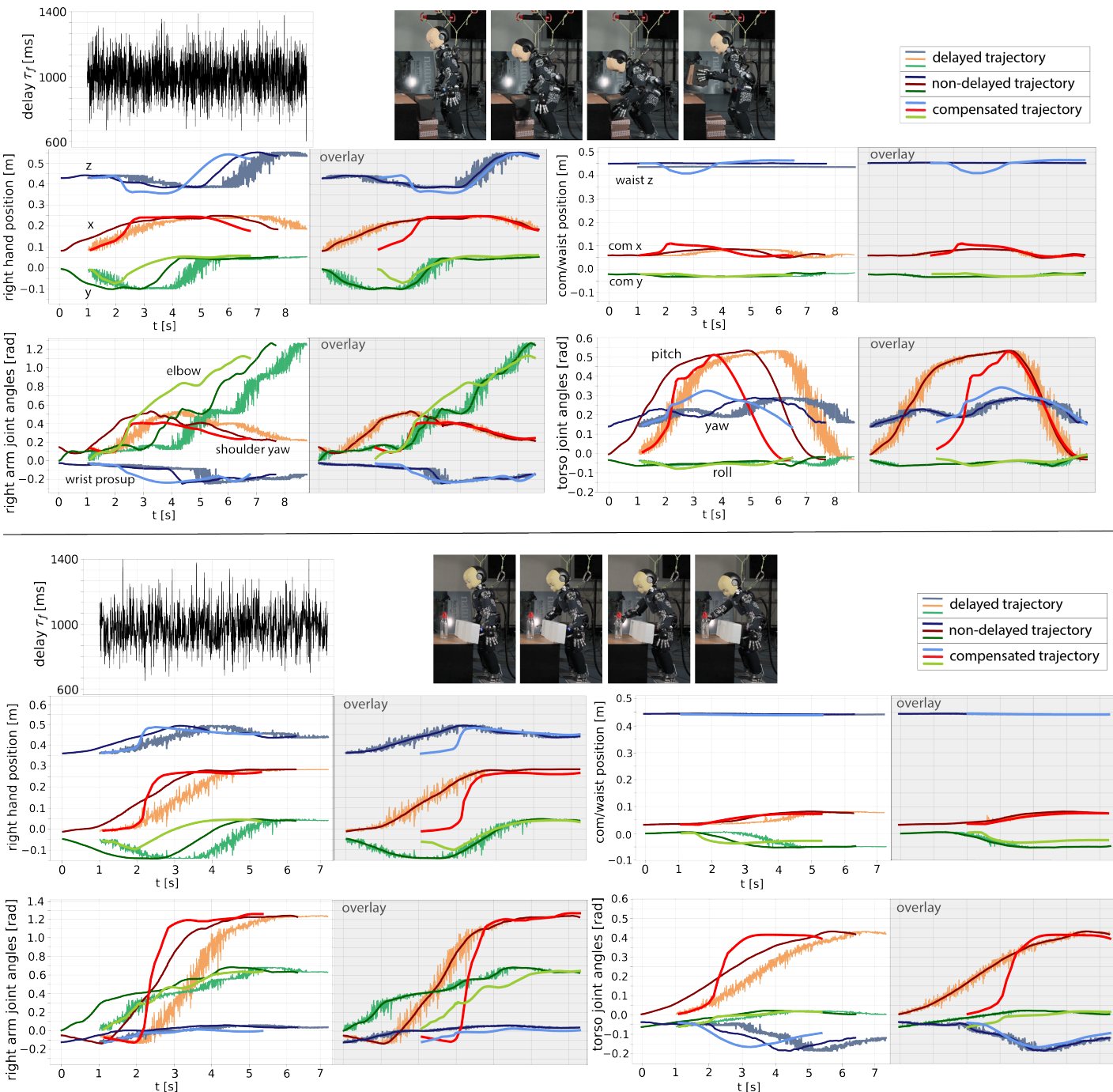
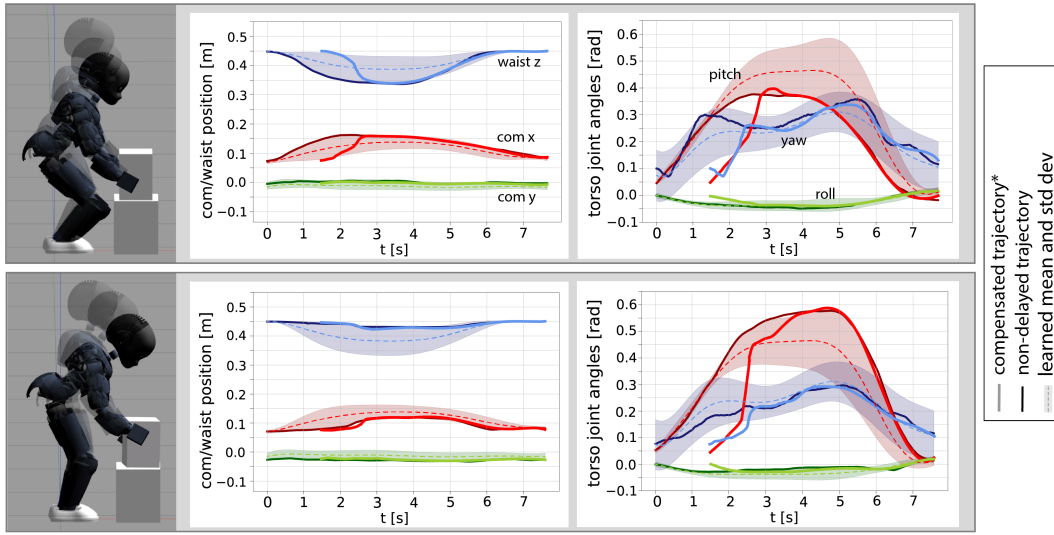
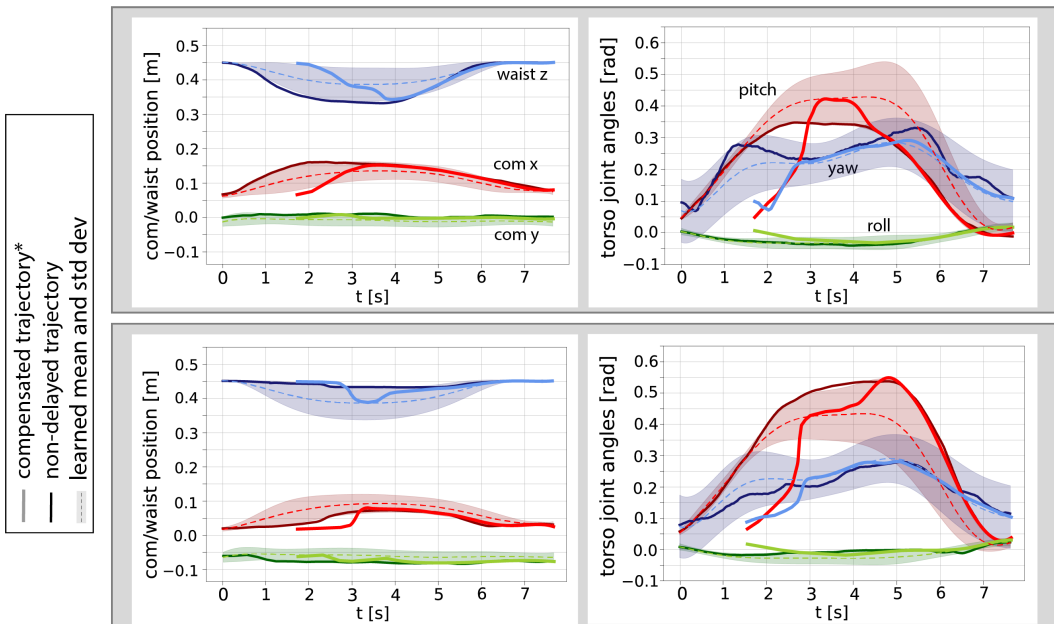


**Fig. S6. Teleoperation with compensation of a round-trip delay around 2s.** Top: The robot is picking up a box in front of it at a low height. Bottom: The robot is reaching a bottle located on the table behind an obstacle. The forward delay is around 1000ms with a jitter of 400ms. First, the robot reference trajectories follow the delayed teleoperated signals, then when the prediction is available, the robot is able to anticipate the teleoperated motion.



\*temporally realigned with the non-delayed (actual retargeted) trajectory for comparison purposes

**Fig. S7. Comparison between the compensated trajectory and the ideal (non-delayed) trajectory with a round-trip of around 1.5 s** After the initial recognition period, our approach makes the robot follow the specific way the human is performing the task despite the delay. This is not the same as following the mean of previously demonstrated motions (here, the dashed line).



\*temporally realigned with the non-delayed (actual retargeted) trajectory for comparison purposes

**Fig. S8. Teleoperation with a round-trip delay around 2s compensated by our approach vs learned trajectories distributions.** For very high delays even the continuous update of the prediction might not be sufficient to make the robot follow the specific way the operator is performing the task. Here, first the robot follows the delayed retargeted movements; then tends to follow the learned mean trajectory during the beginning of the compensation; only toward the end is able to compensate for the delay while following the actual retargeted reference.

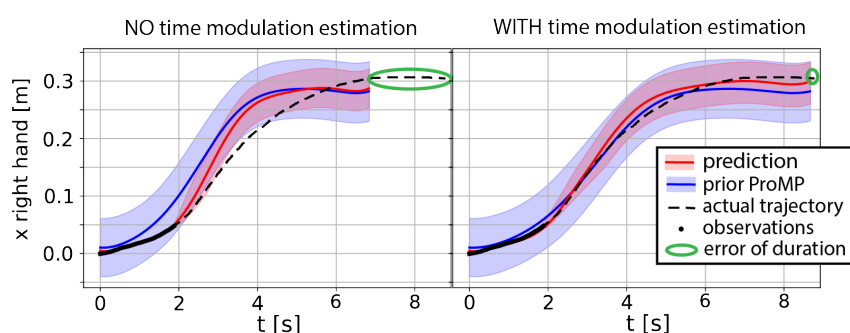


**Fig. S9. Time modulation estimation.** Predicted trajectory given some early observations compared to the actual trajectory, with (right) and without (left) time modulation estimation for the task of reaching a bottle in front of the robot. Without time modulation estimation, the duration of the mean trajectory of a ProMP is set equal to the mean duration of the demonstrations, leading to mismatches between teleoperated (dashed line) and predicted (red line) motion.

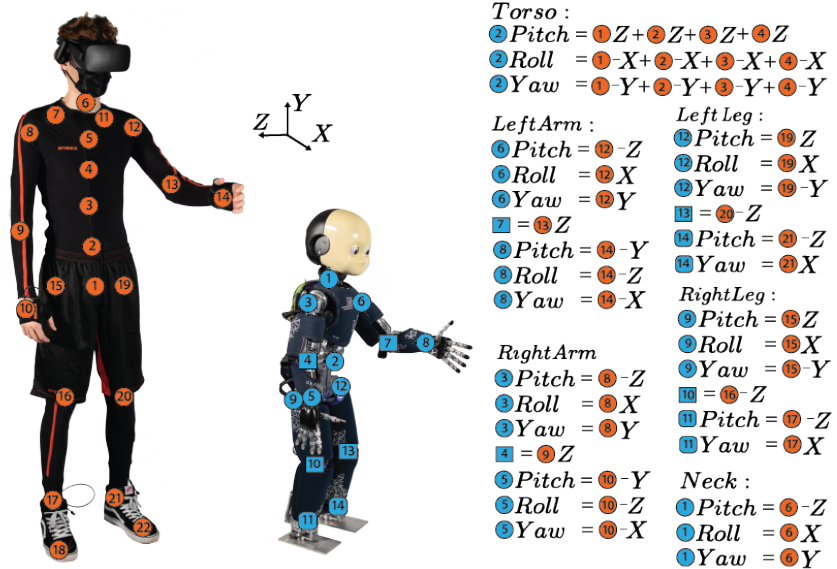


**Fig. S10.** Posture retargeting from human (Xsens system) to iCub. Each joint of the robot is associated to a spherical joint of the Xsens skeleton together with its rotation axis.

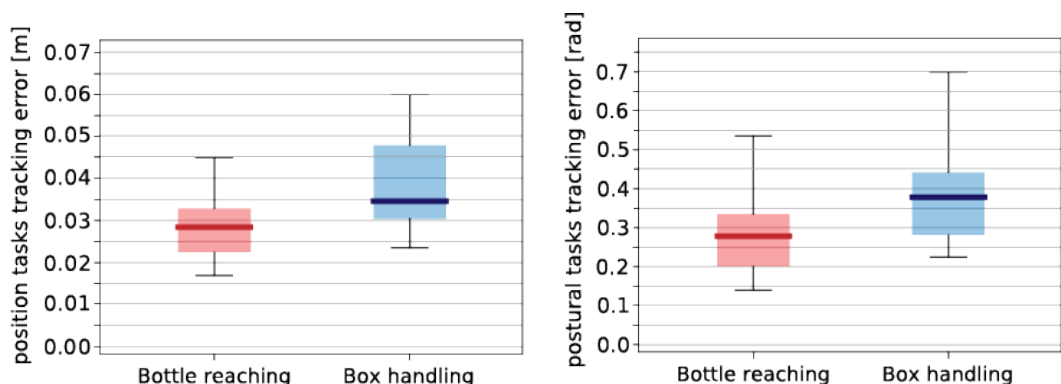


**Fig. S11. Controller tracking error.** Boxplots representing the cumulative tracking error for both the position tasks and the postural tasks of the multi-task controller, in the two main experimental scenarios of reaching a bottle at different locations with the right hand and handling a box, measured while teleoperating the robot during the demonstrations.